Supporting Information

Strong Upconverted Circularly Polarized Emission from a Chiral Tetrahedral Yb/Eu Cage

Zhiwei Yao, Ting Gao, Pengfei Yan, Yanyan Zhou* and Hongfeng Li*

Key Laboratory of Functional Inorganic Material Chemistry, Ministry of Education; School of Chemistry and Materials Science, Heilongjiang University, Harbin 150080, P. R. China
E-mail: zhouyanyan@hlju.edu.cn; lihongfeng@hlju.edu.cn

Table of contents

1. Experimental section

1.1 General

Materials and measurements

Unless otherwise stated, all chemicals and solvents were purchased from commercial companies and used as received. Deuterated solvents were purchased from Energy-Chemical and Macklin. Electrospray time-of-flight (ESI-TOF-MS) mass spectra were recorded on a Bruker maXis mass spectrometer. Data analysis was conducted with the Mass-Lynx Data Analysis software (Version 4.1) and simulations were performed with the MassLynx Isotope Pattern software. The ^{1}H, ^{19}F, ^{31}P, as well as the COSY, NOESY and DOSY spectra, were recorded with a Bruker Avance III 400 MHz spectrometer. The chemical shifts are referenced internally to tetramethylsilane (TMS) or solvents in parts per million (ppm). The ^{1}H NMR spectra assignments were reported as follows (s = singlet, d = doublet, t = triplet, m = multiplet, coupling constant(s) in Hz; integration). The ^{1}H NMR NMR chemical shifts were referenced to the residual signals of the deuterated solvents used ($CDCl_3$, ^{1}H NMR: δ = 7.26 ppm; CD_3OD, ^{1}H NMR: δ = 3.31 ppm). The ^{19}F NMR spectra were referenced to an external standard of 5% TFA (0 ppm) in 0.6 mL D_2O. The ^{31}P NMR spectra were referenced to an external standard of 5% H_3PO_4 (0 ppm) in 0.6 mL D_2O.

The Stokes-Einstein equation:

$$D = \frac{K_B T}{6\pi\eta r}$$

was applied to estimate the dynamic radius for the assemblies. The estimated dynamic radius r was obtained from DOSY spectrum, K_B is Boltzmann constant, T is temperature, η is viscosity of solvent used, and D is diffusion coefficient.

Optical measurements

UV-visible absorption spectra were recorded at room temperature using 1 cm light path quartz cuvettes with a Perkin-Elmer Lambda 25 spectrometer. UV-vis-NIR absorption spectra were measured on a Perkin-Elmer Lambda 750 spectrometer. Excitation and emission spectra were recorded using an Edinburgh FLS 980 fluorescence spectrophotometer equipped with a red-sensitive photomultiplier detector (Hamamatsu R928) and measured with quartz cuvettes of 10 mm path length. Luminescence lifetimes were recorded on a single photon counting spectrometer from Edinburgh Instruments (FLS 980) with a microsecond pulse lamp as the excitation source. The data were analyzed using the software supplied by Edinburgh Instruments. For the upconversion luminescence spectra, a 980 nm continuous-wave laser diode (Product model: MW-GX-980/5000 mW http://www.cc-laser.com) was used as the light source. The dependence of upconversion luminescence intensity on power density was measured by increasing the laser power from 2.01 to 37.43 W/cm^2 (spot size of ~0.13 cm^2) for the sample.

CD and UC-CPL experiments were performed on an Olis DM245 spectrometer at room temperature. CD spectra were measured with quartz cuvettes of 10 mm path length and a slit width of 2 mm in the range of 250−450 nm. UC-CPL spectra were recorded with an external excitation source 980 nm semiconductor laser as light source. The emission of left- and right-handed polarized light were collected in the range of 550−720 nm with the integration time of 1 s and the emission slit width of 0.12 mm. During the measurement of UC-CPL, a 980 nm notch filter or long pass filter is perpendicularly placed between the sample and PEM to filter the residual 980 nm excitation light.

Femtosecond transient absorption (fs-TAS)

The ultrafast fs-TA measurements were conducted on a fs pump-probe system in association with an amplified laser system under ambient conditions, which consist of a modelocked Ti:sapphire seed laser (Spectra Physics, Maitai) directed to a regenerative amplifier (Spitfire Pro, Spectra Physics) and a high power laser (Empower, Spectra Physics) used for pumping and amplifier. The amplified 800 nm output was divided into two parts, and the pump pulses with tunable wavelength were generated by the major part of the beam (~85%) after an optical parametric amplifier (TOPAS prime, Spectra Physics), while the white-light continuum (WLC) probe and reference pulses (420−780 nm) were generated by the rest part of the beam passed through an optical delay line, here, the probe beam travelled through the sample and the reference beam was sent directly to the reference spectrometer. A chopper which can modulate the pump pulses was employed to obtain fs-TA spectra with and without the pump pulses alternately, and an optics fiber coupled to a multichannel spectrometer with a CMOS sensor was used to record the pump-induced fluctuation in probe/reference beam intensity with adjusting the optical delay line (maximum ~ 3 ns). The spectral profiles were further processed by the Surface Xplorer.

X-ray crystallography

X-ray diffraction studies for complexe (Yb_4L_4)(R-BINAPO)$_4$ was performed on a Xcalibur, Eos, diffractometer using Mo Kα radiation (λ = 0.71073 Å) under 100 K. Data reduction was done with the CrysAlisPro package.[1] Crystallographic data are given in Tables S1. The structures were solved by direct methods and refined by full-matrix least-squares on *F2* with anisotropic displacement using the SHELXL 2014 program[2] in the Olex2 package.[3] Due to the large number of amorphous solvents and highly-disordered counterions in the unit cell, the residual electron intensities were handled by the PLATON/SQUEEZE routine.[4] The crystallographic data in CIF format were deposited at the Cambridge Crystallographic Data Centre with CCDC No. 2416911. These data are available free of charge from the Cambridge Crystallographic Data Centre, 12 Union Road, Cambridge CB21 EZ, UK; Fax :(+44) 1223−336033 or e-mail: deposit@ccdc.cam.ac.uk.

1.2 Synthetic of complexes

Synthesis of chiral tetrahedral cage Ln_4L_4(R-BINAPO)$_4$. Ligand **L** (0.20 g, 0.30 mmol) and NEt_3 (0.09 g, 0.90 mmol) were dissolved in MeOH, and the mixture was allowed to stir for 5 min. To this solution, $LnCl_3 \cdot 6H_2O$ (0.30 mmol), and (R)-BINAPO (0.20 g, 0.30 mmol) were added dropwise and stirred overnight at room temperature. The product was filtered and dried under vacuum to give the desired product, crystals were obtained by slow diffusion of n-hexane into THF solution of the complex.

Yb_4L_4(R-BINAPO)$_4$. Yield: 80.5%. ^{1}H NMR (400 MHz, $CDCl_3$, 298 K) δ = 10.50−8.84 (m, 34H), 8.76−7.42 (m, 98H), 7.87−7.10 (m, 128H). ^{19}F NMR (376 MHz, $CDCl_3$, 298 K) δ = −9.08 ppm. ^{31}P NMR (162 MHz, $CDCl_3$, 298 K) δ = 30.09 ppm.
Lu_4L_4(R-BINAPO)$_4$. Yield: 79.5%. ^{1}H NMR (400 MHz, $CDCl_3$, 298 K) δ = 7.95−7.82 (m, 16H), 7.67−7.59 (d, *J* = 6.4 Hz, 24H), 7.58−7.49 (m, 16H), 7.44−7.34 (m, 24H), 7.34−7.27 (t, *J* = 8.0 Hz, 16H), 7.19−5.99 (m, 56H), 7.03−6.94 (m, 8H), 6.90−6.77 (m, 16H), 6.76−6.69 (d, *J* = 8.4 Hz, 24H), 6.66−6.54 (m, 16H), 6.22 ppm (s, 12H). ^{19}F NMR (376 MHz, $CDCl_3$, 298 K) δ = 1.145 ppm. ^{31}P NMR (162 MHz, $CDCl_3$, 298 K) δ = 31.75 ppm.

Synthesis of chiral tetrahedral cages ($Yb_xEu_{4-x}L_4$)(R/S-BINAPO)$_4$ (x = 0−3.5). Ligand L (0.20 g, 0.30 mmol) and NEt_3 (0.09 g, 0.90 mmol) were dissolved in MeOH, and the mixture was allowed to stir for 5 min. To this solution, $EuCl_3 \cdot 6H_2O$ (0.30 mmol), $YbCl_3 \cdot 6H_2O$ (0.30−a mmol) and R/S-BINAPO (0.20 g, 0.30 mmol) were added dropwise and stirred overnight at room temperature. The product was filtered and dried under vacuum to give the desired product. We successfully synthesized seven variations of the chiral tetrahedral cages ($Yb_{0.5}Eu_{3.5}L_4$)(R/S-BINAPO)$_4$, ($Yb_{1.0}Eu_{3.0}L_4$)(R/S-BINAPO)$_4$, ($Yb_{1.5}Eu_{2.5}L_4$)(R/S-BINAPO)$_4$, ($Yb_{2.0}Eu_{2.0}L_4$)(R/S-BINAPO)$_4$, ($Yb_{2.5}Eu_{1.5}L_4$)(R/S-BINAPO)$_4$, ($Yb_{3.0}Eu_{1.0}L_4$)(R/S-BINAPO)$_4$, and ($Yb_{3.5}Eu_{0.5}L_4$)(R/S-BINAPO)$_4$.

($Yb_{0.5}Eu_{3.5}L_4$)(R-BINAPO)$_4$. Yield: 78.5%. ^{1}H NMR (400 MHz, CD_3OD, 298 K) δ = 11.58−10.74 (m, 24H), 8.13−7.86 (m, 24H), 7.83−7.62 (m, 24H), 7.61−7.14 (m, 106H), 6.89−6.53 (d, *J* = 60 Hz, 24H). ^{19}F NMR (376 MHz, CD_3OD, 298 K) δ = −0.45, −5.89, −17.06 ppm. ^{31}P NMR (162 MHz, CD_3OD, 298 K) δ = 31.75 ppm.
($Yb_{1.0}Eu_{3.0}L_4$)(R-BINAPO)$_4$. Yield: 77.0%. ^{1}H NMR (400 MHz, CD_3OD, 298 K) δ = 11.23−10.48 (m, 22H), 8.08−7.87 (m, 24H), 7.81−7.63 (m, 24H), 7.59−7.31 (m, 104H), 6.93−6.55 (m, 24H). ^{19}F NMR (376 MHz, CD_3OD, 298 K) δ = −0.45, −5.89, −17.06 ppm. ^{31}P NMR (162 MHz, CD_3OD, 298 K) δ = 31.75 ppm.
($Yb_{1.5}Eu_{2.5}L_4$)(R-BINAPO)$_4$. Yield: 79.7%. ^{1}H NMR (400 MHz, CD_3OD, 298 K) δ = 10.35−9.51 (m, 24H), 8.07−7.87 (m, 24H), 7.82−7.65 (m, 24H), 7.63−7.32 (m, 102H), 6.93−6.60 (m, 22H). ^{19}F NMR (376 MHz, CD_3OD, 298 K) δ = −0.45, −5.89, −17.06 ppm. ^{31}P NMR (162 MHz, CD_3OD, 298 K) δ = 31.75 ppm.
($Yb_{2.0}Eu_{2.0}L_4$)(R-BINAPO)$_4$. Yield: 75.6%. ^{1}H NMR (400 MHz, CD_3OD, 298 K) δ = 10.91−9.70 (m, 28H), 8.06−7.84 (m, 24H), 7.80−7.62 (m, 22H), 7.62−7.26 (m, 82H), 6.96−6.51 (d, *J* = 60 Hz, 16H). ^{19}F NMR (376 MHz, CD_3OD, 298 K) δ = −0.45, −5.89, −17.06 ppm. ^{31}P

NMR (162 MHz, CD_3OD, 298 K) δ = 31.75 ppm.

$(Yb_{2.5}Eu_{1.5}L_4)$(R-BINAPO)$_4$. Yield: 77.8%. ICP analysis: calcd (62.50% Yb: 37.50% Eu); obtained (61.44% Yb: 38.56% Eu). ^{1}H NMR (400 MHz, CD_3OD, 298 K) δ = 11.13−9.91 (m, 24H), 8.01−7.84 (m, 24H), 7.83−7.62 (m, 24H), 7.54−7.26 (m, 134H), 6.88−6.58 (m, 30H). ^{19}F NMR (376 MHz, CD_3OD, 298 K) δ = −0.45, −5.89, −17.06 ppm. ^{31}P NMR (162 MHz, CD_3OD, 298 K) δ = 31.75 ppm.

$(Yb_{3.0}Eu_{1.0}L_4)$(R-BINAPO)$_4$. Yield: 75.2%. ^{1}H NMR (400 MHz, CD_3OD, 298 K) δ = 10.67−9.94 (m, 20H), 8.39 (s, 8H), 8.04−7.84 (m, 24H), 7.79–7.62 (m, 18H), 7.58–7.28 (m, 108H), 6.91–6.60 (m, 18H). ^{19}F NMR (376 MHz, CD_3OD, 298 K) δ = −0.45, −5.89, −17.06 ppm. ^{31}P NMR (162 MHz, CD_3OD, 298 K) δ = 31.75 ppm.

$(Yb_{3.5}Eu_{0.5}L_4)$(R-BINAPO)$_4$. Yield: 78.8%. ^{1}H NMR (400 MHz, CD_3OD, 298 K) δ = 10.07−9.74 (m, 20H), 8.37−8.14 (m, 24H), 8.01−7.85 (m, 32H), 7.59−7.25 (d, 188H), 6.89−6.62 (m, 36H). ^{19}F NMR (376 MHz, CD_3OD, 298 K) δ = −0.45, −5.89, −17.06 ppm. ^{31}P NMR (162 MHz, CD_3OD, 298 K) δ = 31.75 ppm.

$(Yb_{2.5}Gd_{1.5}L_4)$(R-BINAPO)$_4$. Yield: 76.3%. ICP analysis: calcd (62.50% Yb: 37.50% Gd); obtained (63.25% Yb: 36.75% Gd).

1.3 Characterization of complexes

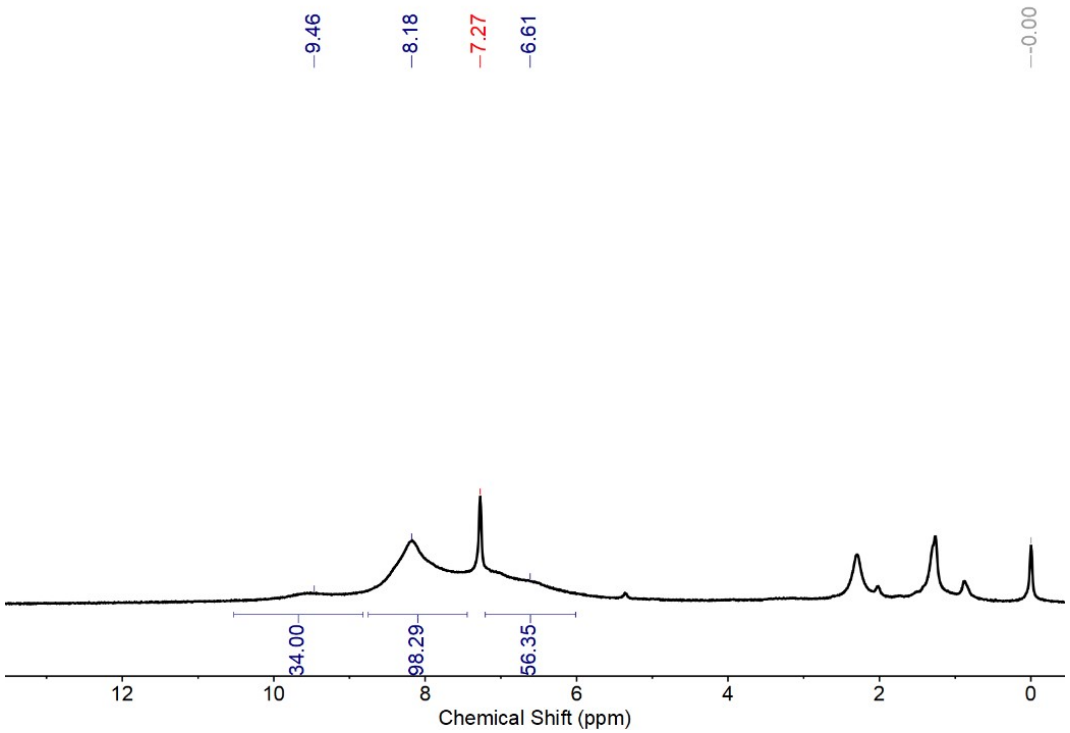

Figure S1. ^{1}H NMR spectrum (400 MHz, 298 K) of $Yb_4\mathbf{L}_4$(R-BINAPO)$_4$ in $CDCl_3$.

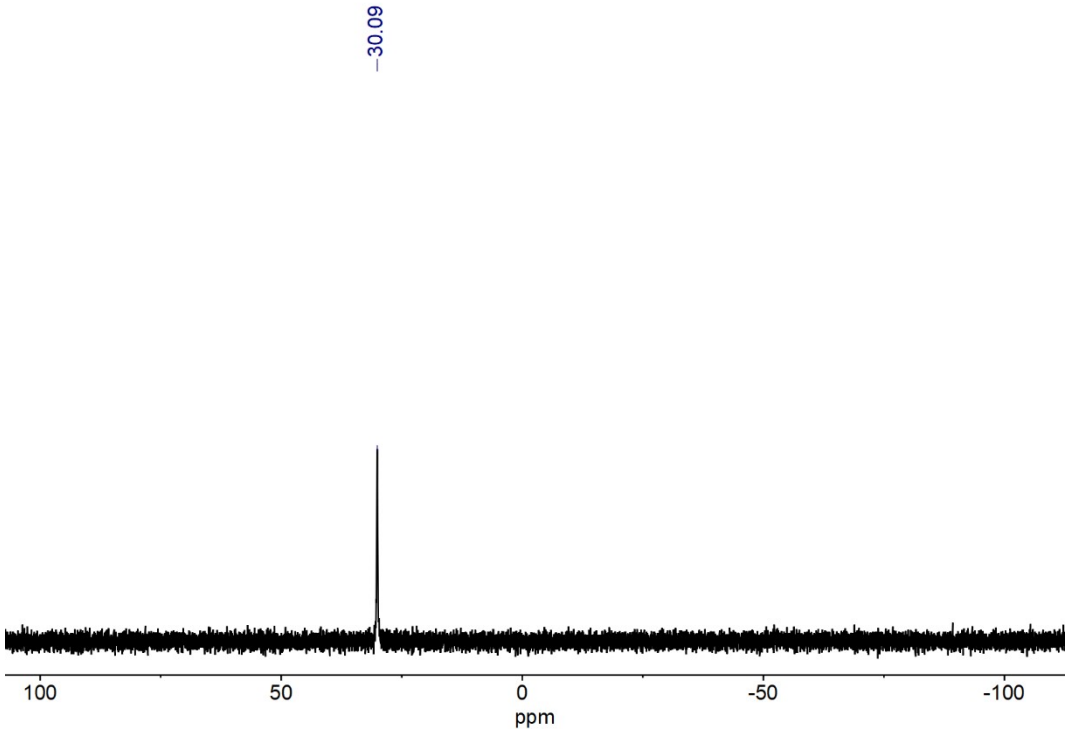

Figure S2. ^{31}P NMR spectrum of ($Yb_4\mathbf{L}_4$)(R-BINAPO)$_4$ in $CDCl_3$ at 298 K.

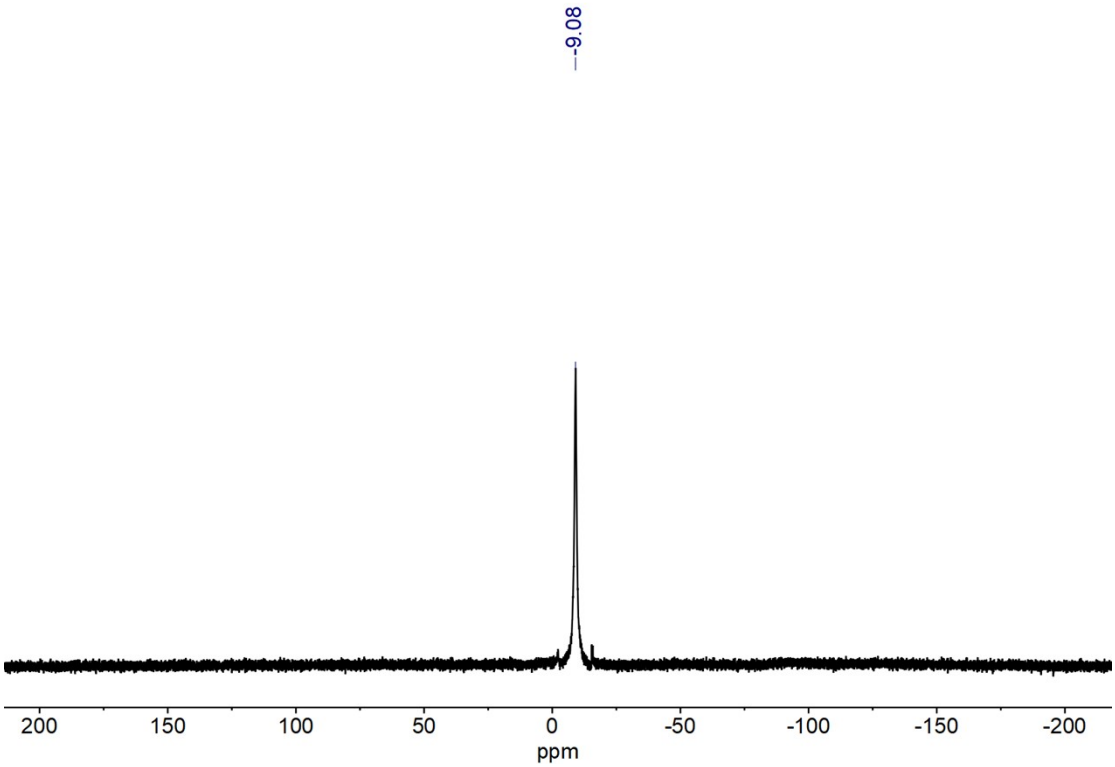

Figure S3. ^{19}F NMR spectrum of $(Yb_4\mathbf{L}_4)(R\text{-}BINAPO)_4$ in $CDCl_3$ at 298 K.

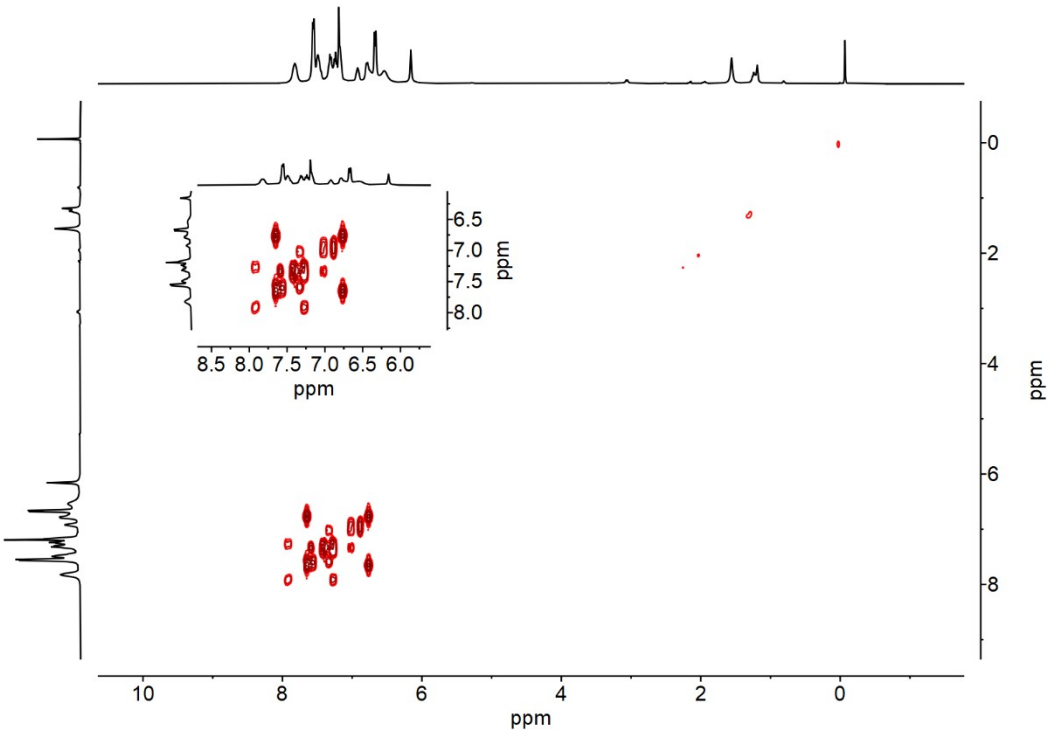

Figure S4. ^{1}H- ^{1}H COSY spectrum of $Lu_4\mathbf{L}_4(R\text{-}BINAPO)_4$ in $CDCl_3$ at 298 K.

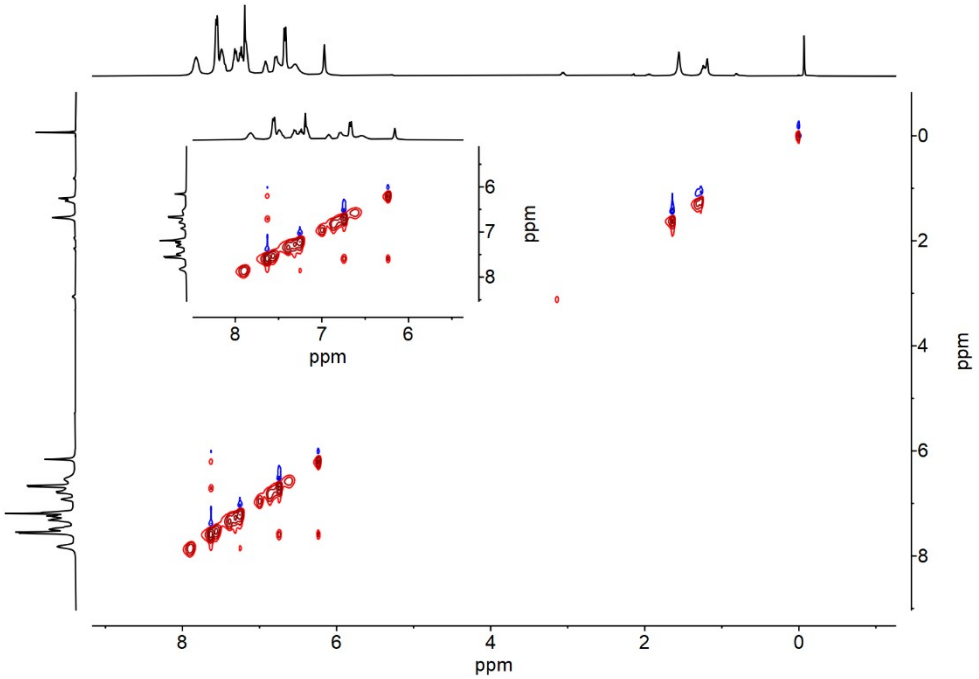

Figure S5. ^{1}H- ^{1}H NOESY spectrum of $Lu_4\mathbf{L}_4$(R-BINAPO)$_4$ in $CDCl_3$ at 298 K.

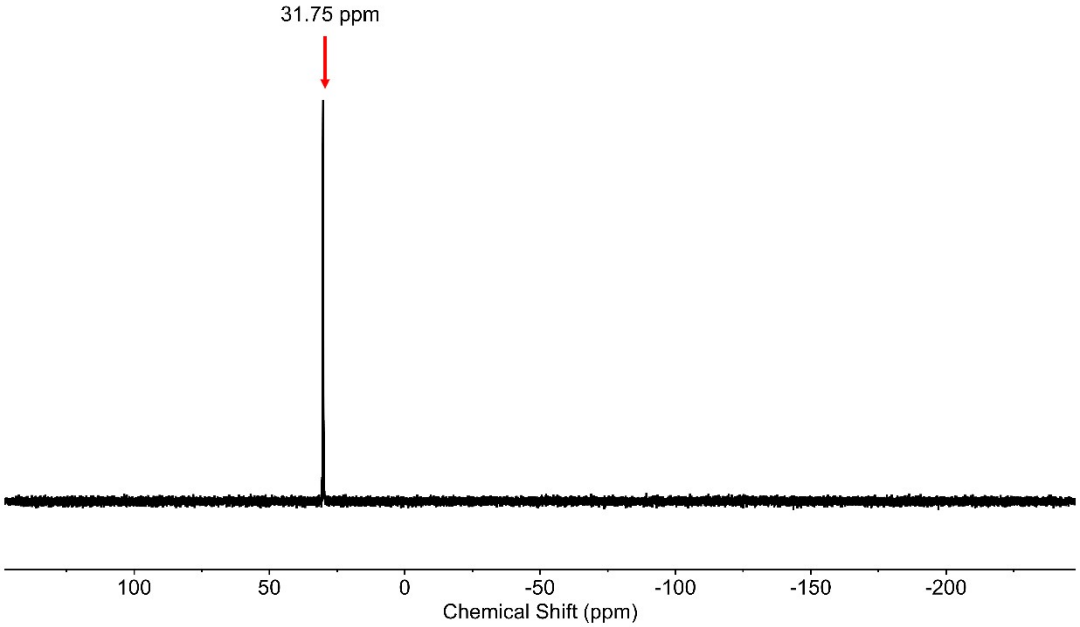

Figure S6. ^{31}P NMR spectrum of $Lu_4\mathbf{L}_4$(R-BINAPO)$_4$ in $CDCl_3$ at 298 K.

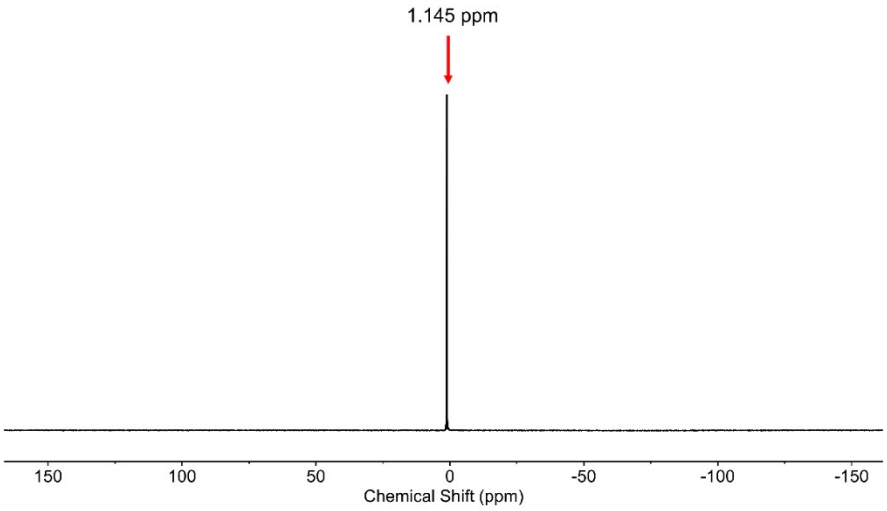

Figure S7. ^{19}F NMR spectrum of $Lu_4\mathbf{L}_4$(R-BINAPO)$_4$ in $CDCl_3$ at 298 K.

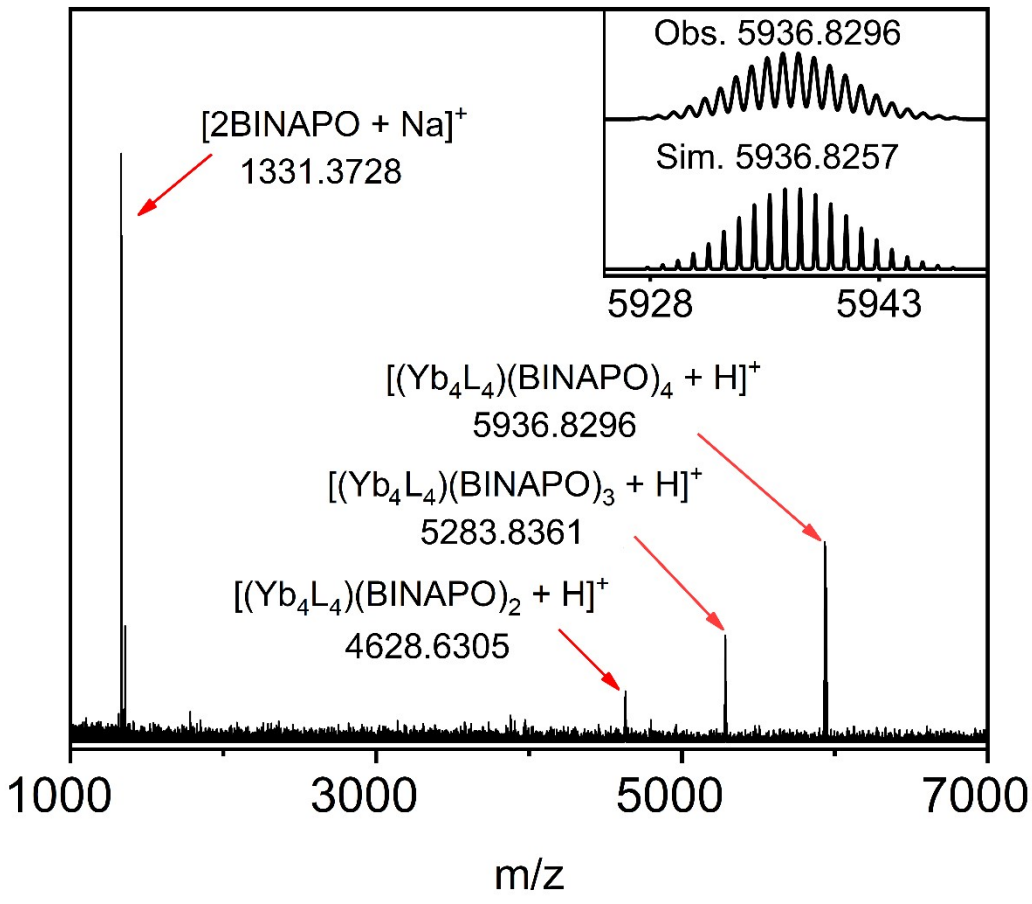

Figure S8. ESI-TOF-MS spectrum of $Yb_4\mathbf{L}_4$(R-BINAPO)$_4$.

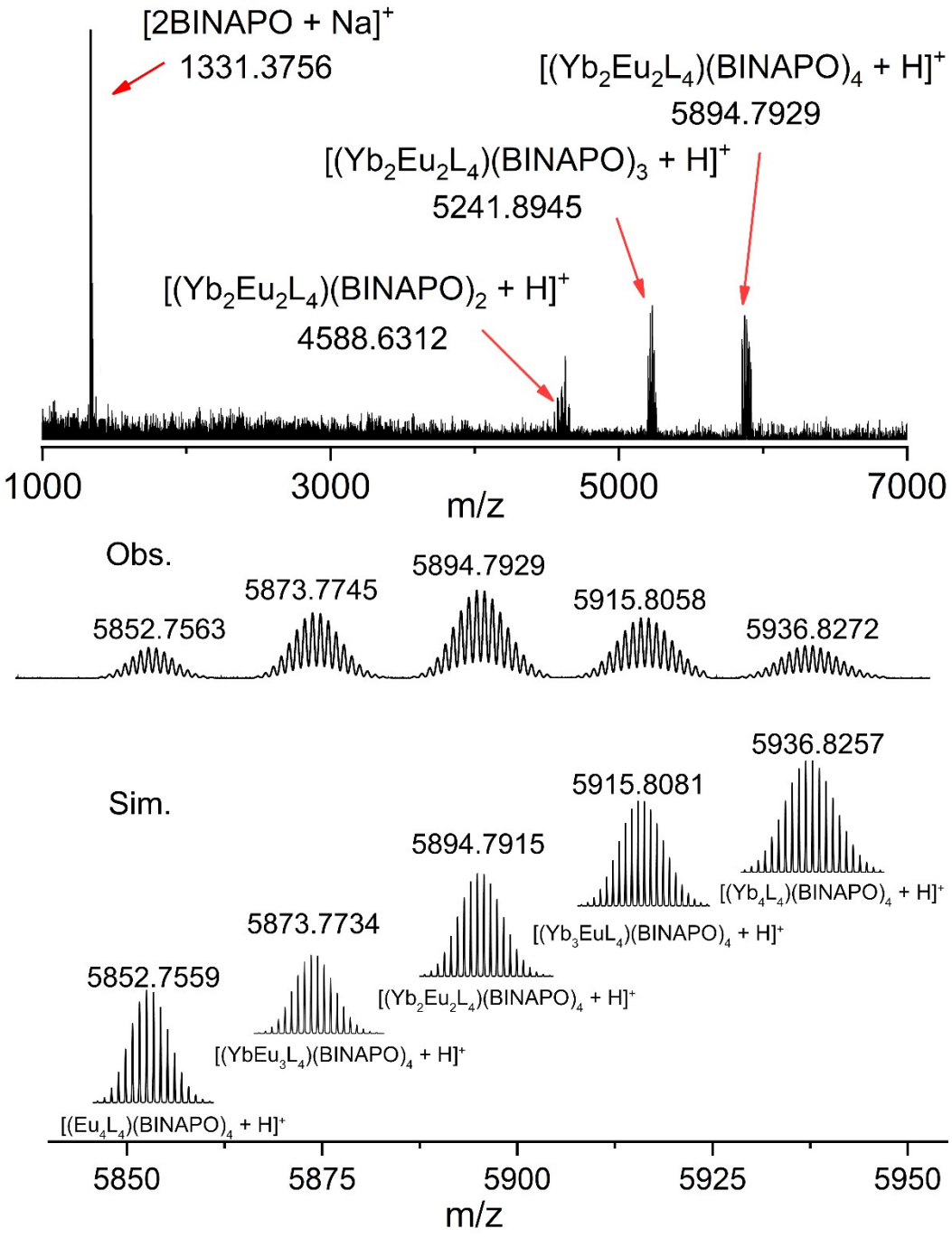

Figure S9. ESI-TOF-MS spectrum of $(Yb_xEu_{4-x}\mathbf{L}_4)(R\text{-BINAPO})_4$.

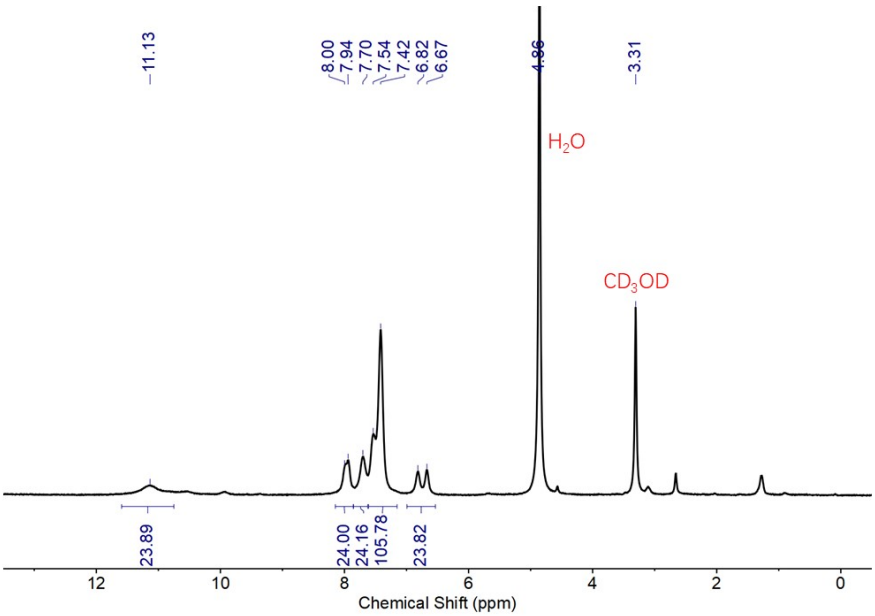

Figure S10. ^{1}H NMR spectrum (400 MHz, 298 K) of $(Yb_{3.5}Eu_{0.5}\mathbf{L}_4)$(R-BINAPO)$_4$ in CD_3OD.

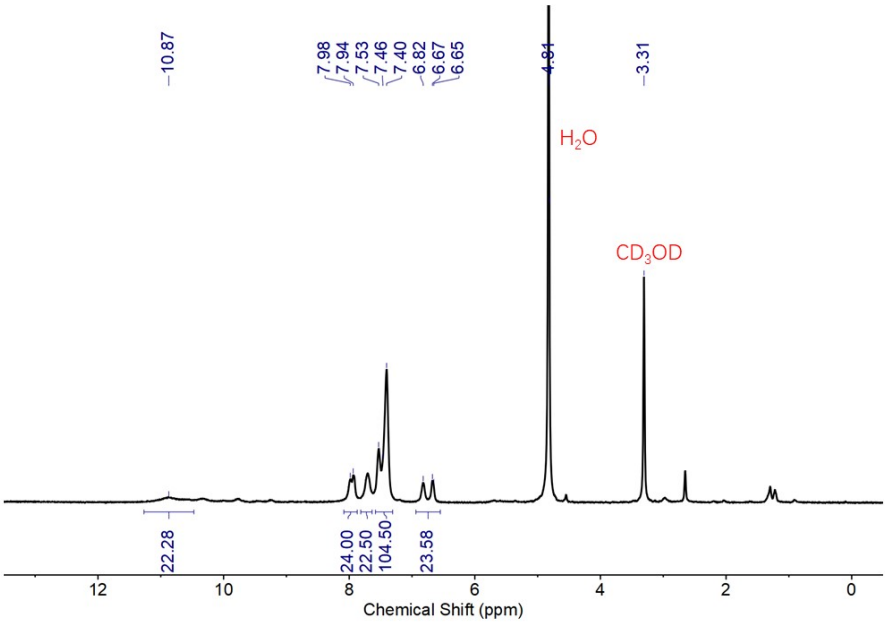

Figure S11. ^{1}H NMR spectrum (400 MHz, 298 K) of $(Yb_{3.0}Eu_{1.0}\mathbf{L}_4)$(R-BINAPO)$_4$ in CD_3OD.

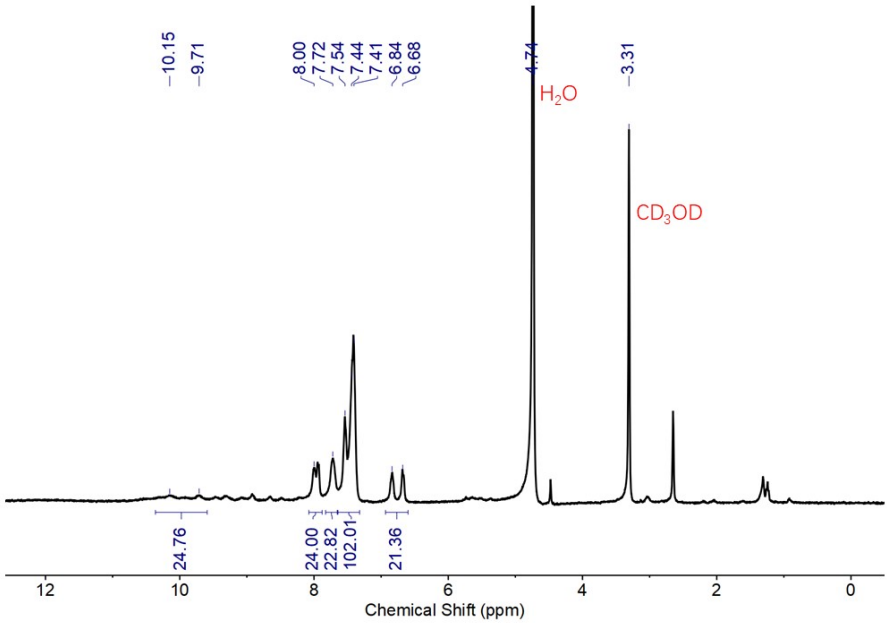

Figure S12. ^{1}H NMR spectrum (400 MHz, 298 K) of $(Yb_{2.5}Eu_{1.5}\mathbf{L}_4)(R\text{-BINAPO})_4$ in CD_3OD.

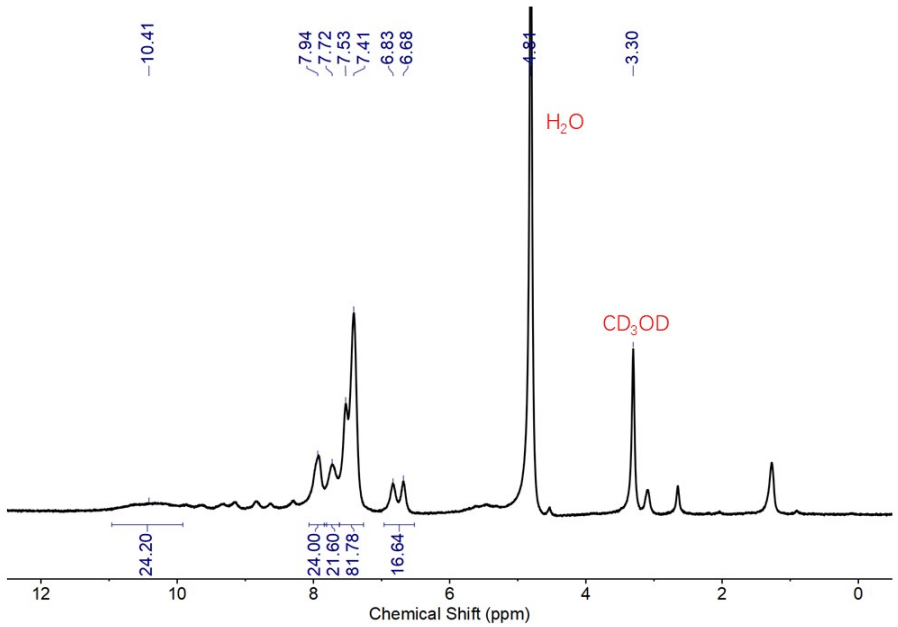

Figure S13. ^{1}H NMR spectrum (400 MHz, 298 K) of $(Yb_{2.0}Eu_{2.0}\mathbf{L}_4)(R\text{-BINAPO})_4$ in CD_3OD.

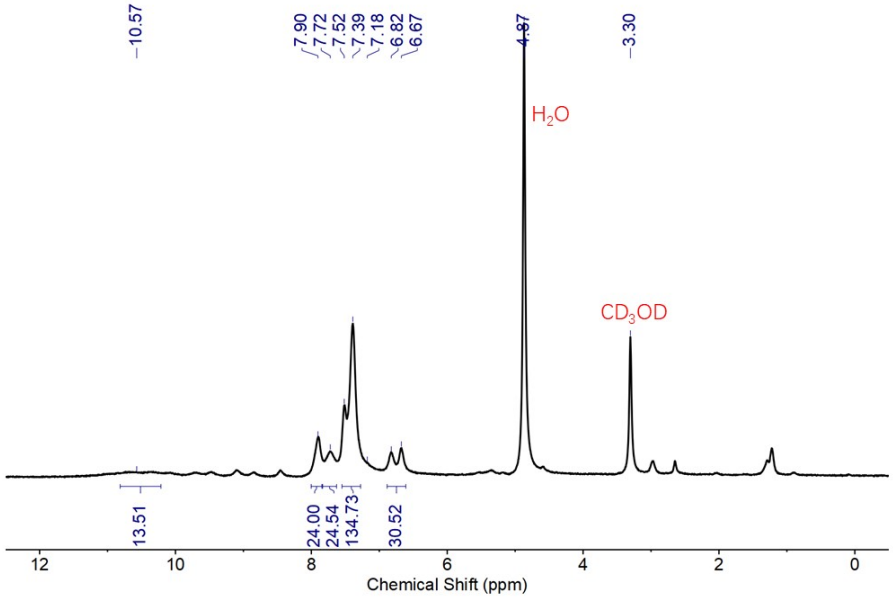

Figure S14. ^{1}H NMR spectrum (400 MHz, 298 K) of $(Yb_{1.5}Eu_{2.5}\mathbf{L}_4)(R\text{-BINAPO})_4$ in CD_3OD.

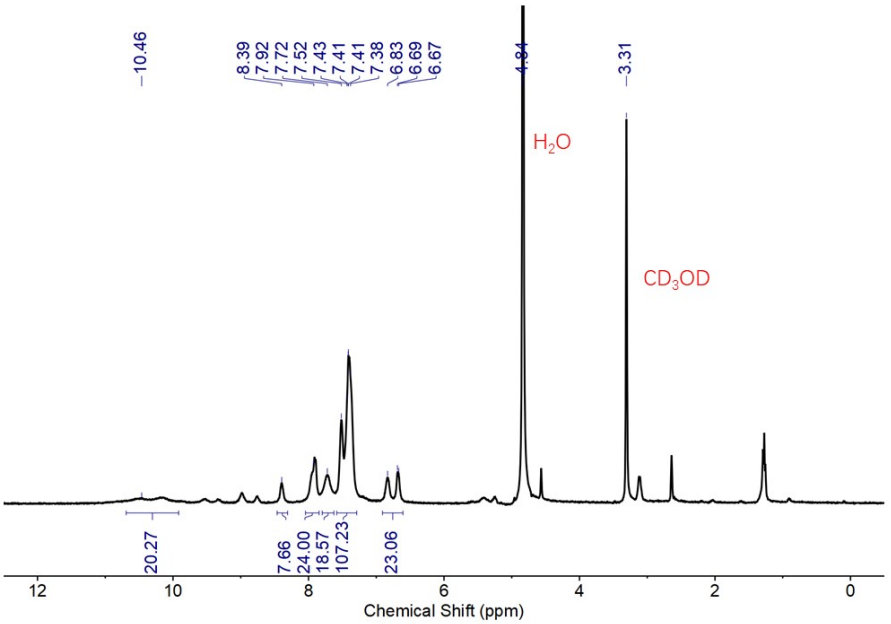

Figure S15. ^{1}H NMR spectrum (400 MHz, 298 K) of $(Yb_{1.0}Eu_{3.0}\mathbf{L}_4)(R\text{-BINAPO})_4$ in CD_3OD.

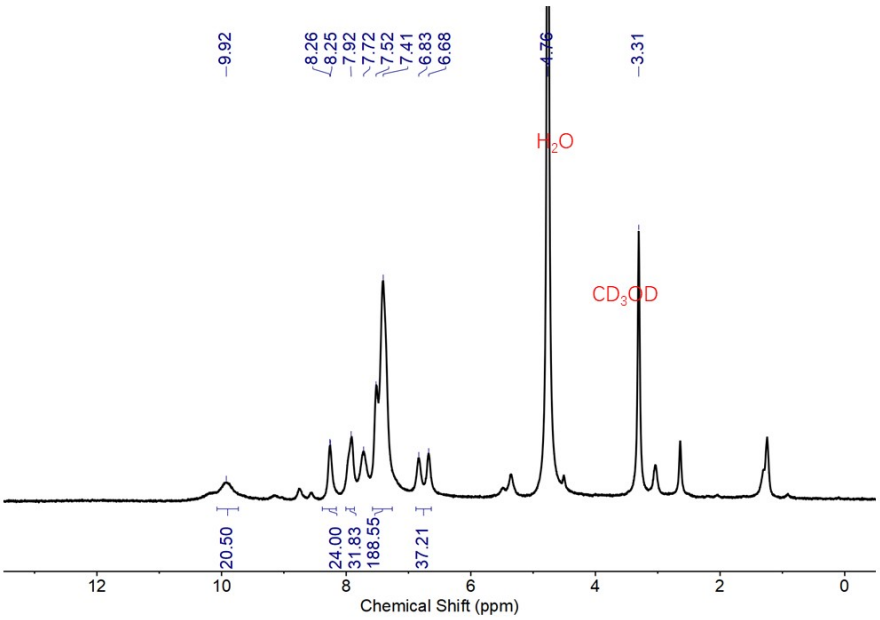

Figure S16. ^{1}H NMR spectrum (400 MHz, 298 K) of $(Yb_{0.5}Eu_{3.5}\mathbf{L}_4)(R\text{-BINAPO})_4$ in CD_3OD.

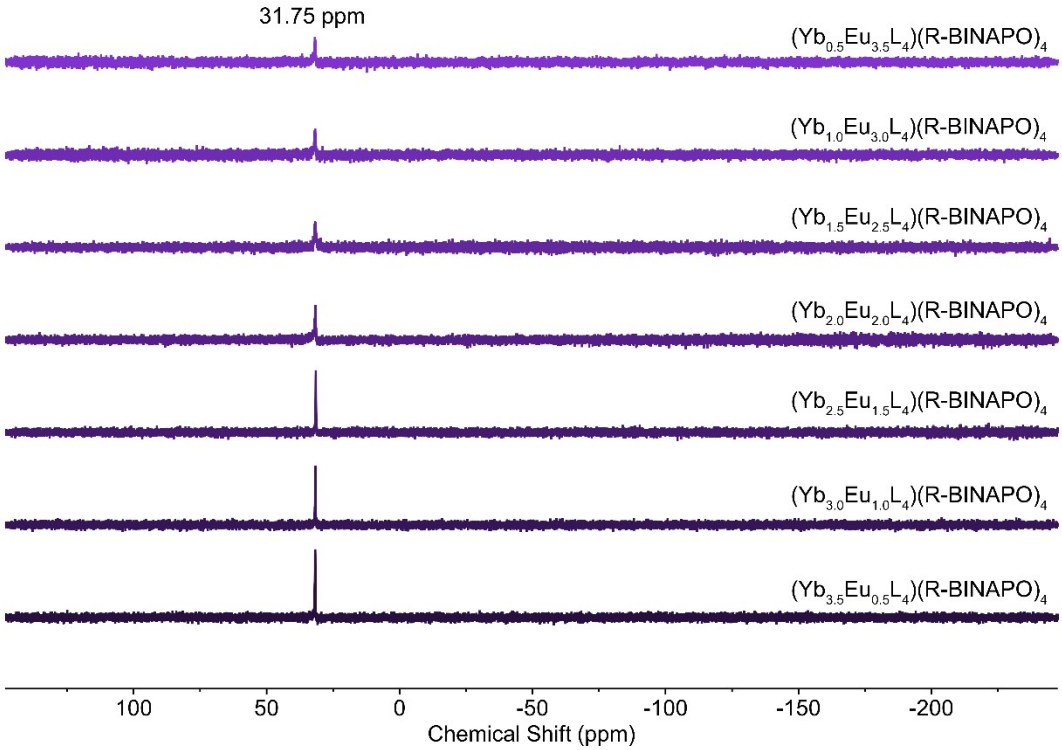

Figure S17. ^{31}P NMR spectra of $(Yb_xEu_{4-x}\mathbf{L}_4)(R\text{-BINAPO})_4$ (x = 0.5−3.5) in CD_3OD at 298K.

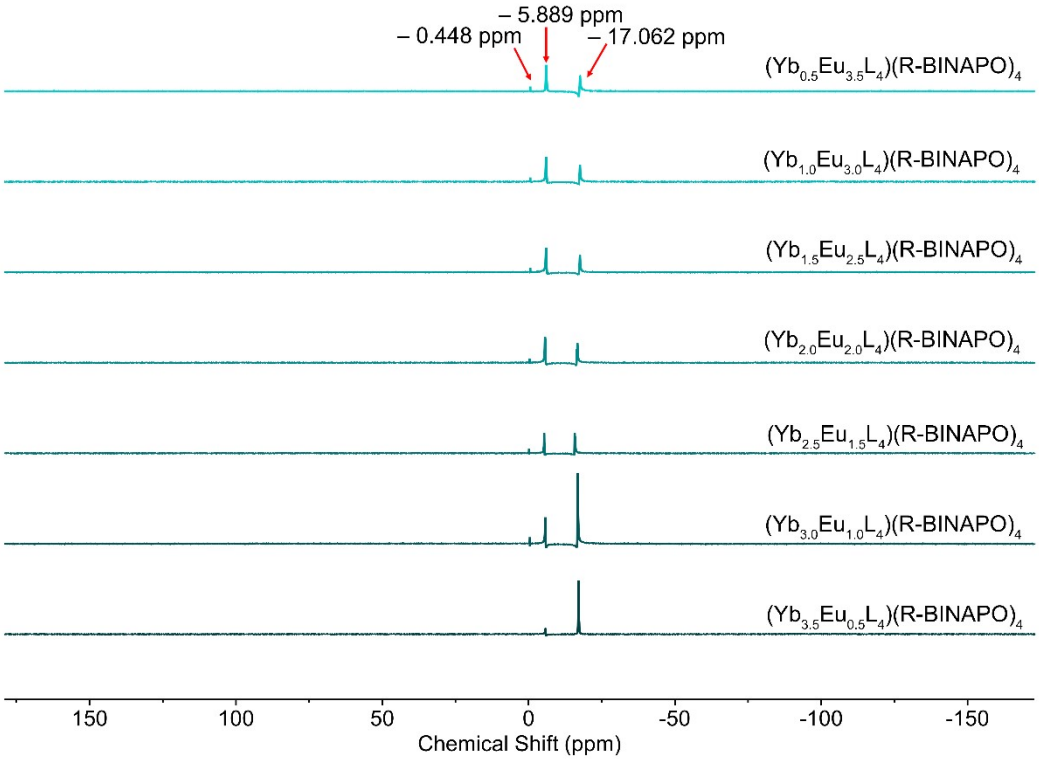

Figure S18. ^{19}F NMR spectra of $(Yb_xEu_{4-x}\mathbf{L}_4)(R\text{-BINAPO})_4$ (x = 0.5−3.5) in CD_3OD at 298K.

2. X-ray crystallography

Table S1. Crystal data and structure refinement for $(Yb_4\mathbf{L}_4)(R\text{-BINAPO})_4$.

Empirical formula	$C_{412}H_{424}Yb_4F_{36}N_4O_{58}P_8$
Formula weight	7983.45
Temperature	100(2) K
Wavelength	0.71073
Crystal system	monoclinic
Space group	C_2
Unit cell dimensions	a = 43.1068(13) Å α = 90°
	b = 21.1124(5) Å β = 129.292(2)°
	c = 29.4778(9) Å γ = 90°
Volume	20762.5(11) Å^3
Z	2
Density	1.277 g/cm^3
Absorption coefficient	1.007 mm^{-1}
F(000)	8224.0
Crystal size	0.21 × 0.20 × 0.16 mm^3
2Θ range for data collection	5.062 to 55.09°
Index ranges	-56 ≤ h ≤ 56, -27 ≤ k ≤ 27, -38 ≤ l ≤ 38
Reflections collected	626320
Independent reflections	47768 [R_{int} = 0.0626, R_{sigma} = 0.0331]
Data / restraints / parameters	47768/2362/3076
Goodness-of-fit on F^2	1.045
Final R indices [I>2sigma(I)]	R_1 = 0.0308, wR_2 = 0.0754
R indices (all data)	R_1 = 0.0381, wR_2 = 0.0793
Flack parameter	-0.0105(12)
Mean I/sig	5.611
Largest diff. peak and hole	1.08/-0.52 e Å^{-3}

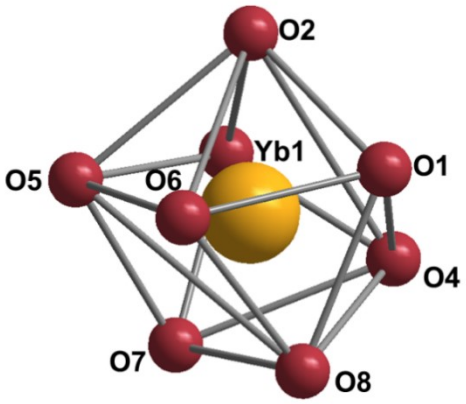

Figure S19. Coordination polyhedra of $Yb_4\mathbf{L}_4(R\text{-BINAPO})_4$.

3. Photophysical properties

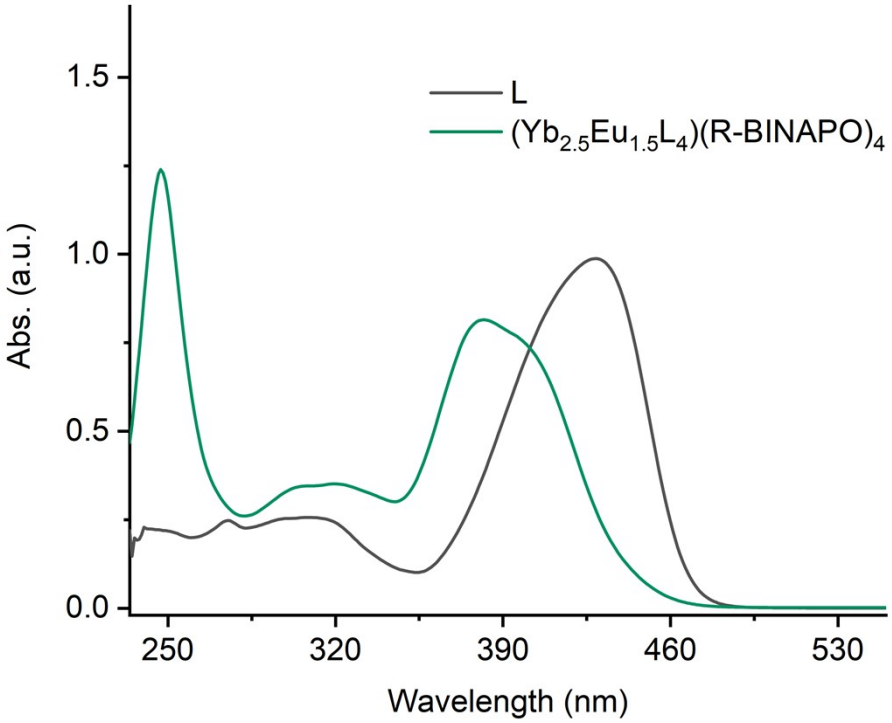

Figure S20. UV-visible absorption spectra of free ligand **L** (c = 1.0 × 10^{-5} M) and $(Yb_{2.5}Eu_{1.5}L_4)(R\text{-}BINAPO)_4$ (c = 2.5 × 10^{-6} M) in $CHCl_3$.

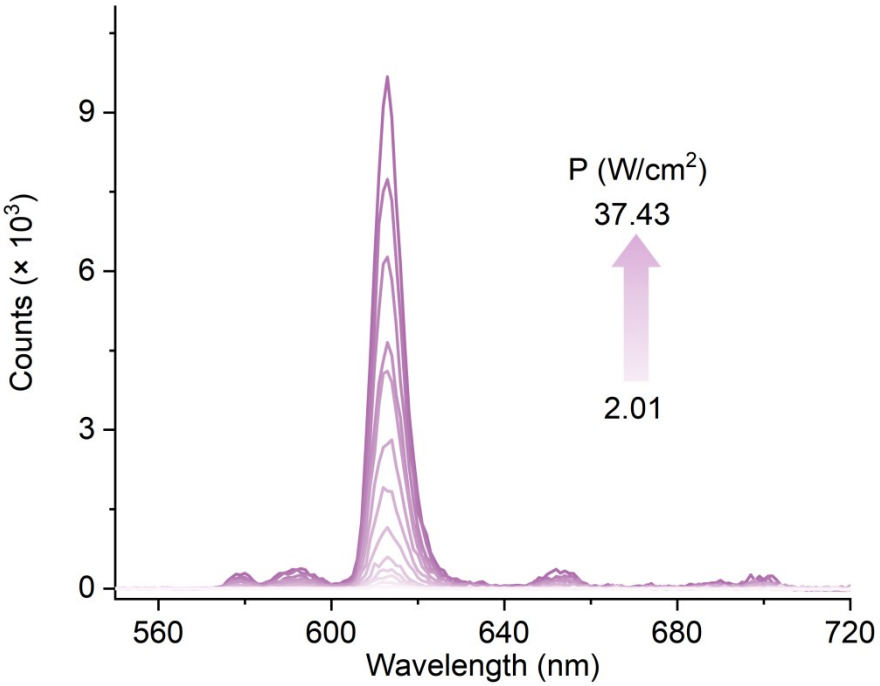

Figure S21. The UC emission spectra of $(Yb_{1.5}Eu_{2.5}\mathbf{L}_4)(R\text{-}BINAPO)_4$ in $CHCl_3$ with variable laser power (λ_{ex} = 980 nm, c = 2.5 × 10^{-3} M, Number of scans = 1).

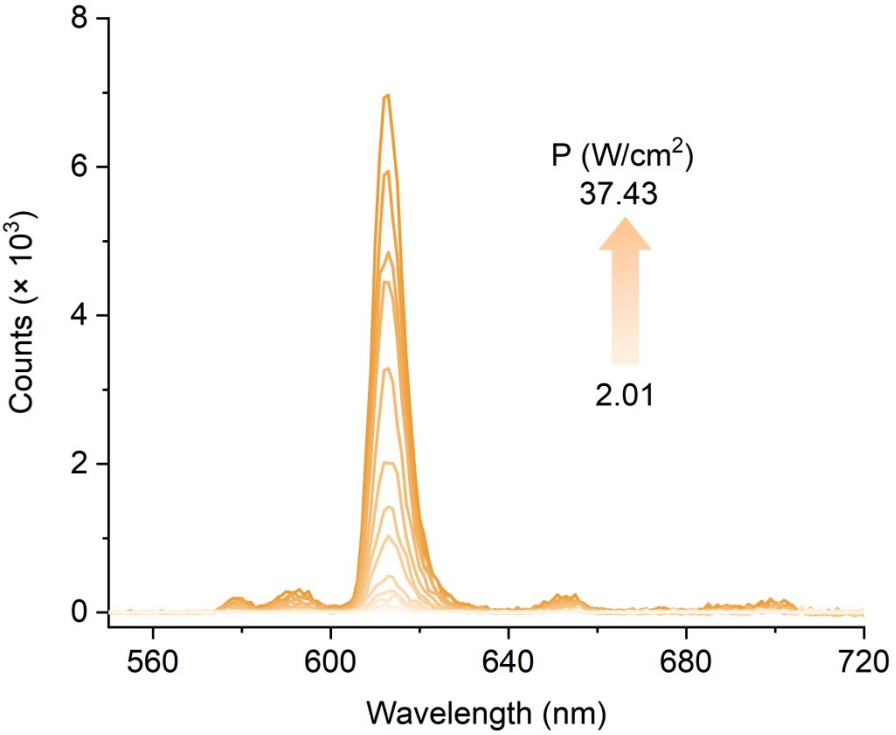

Figure S22. The UC emission spectra of $(Yb_{3.0}Eu_{1.0}\mathbf{L}_4)(R\text{-}BINAPO)_4$ in $CHCl_3$ with variable laser power (λ_{ex} = 980 nm, $c = 2.5 \times 10^{-3}$ M, Number of scans = 1).

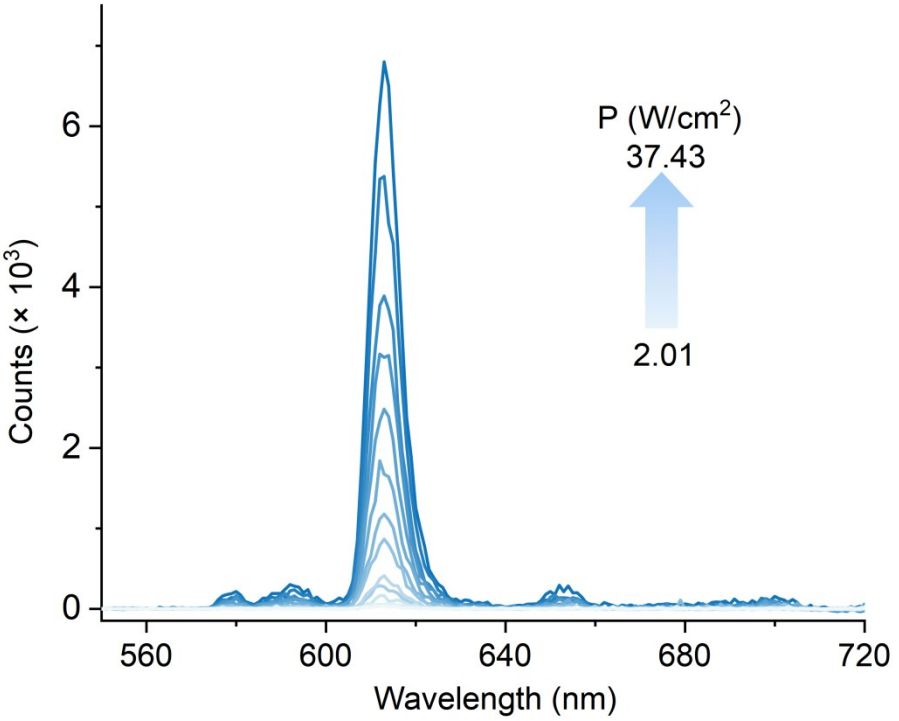

Figure S23. The UC emission spectra of $(Yb_{2.0}Eu_{2.0}\mathbf{L}_4)(R\text{-}BINAPO)_4$ in $CHCl_3$ with variable laser power (λ_{ex} = 980 nm, $c = 2.5 \times 10^{-3}$ M, Number of scans = 1).

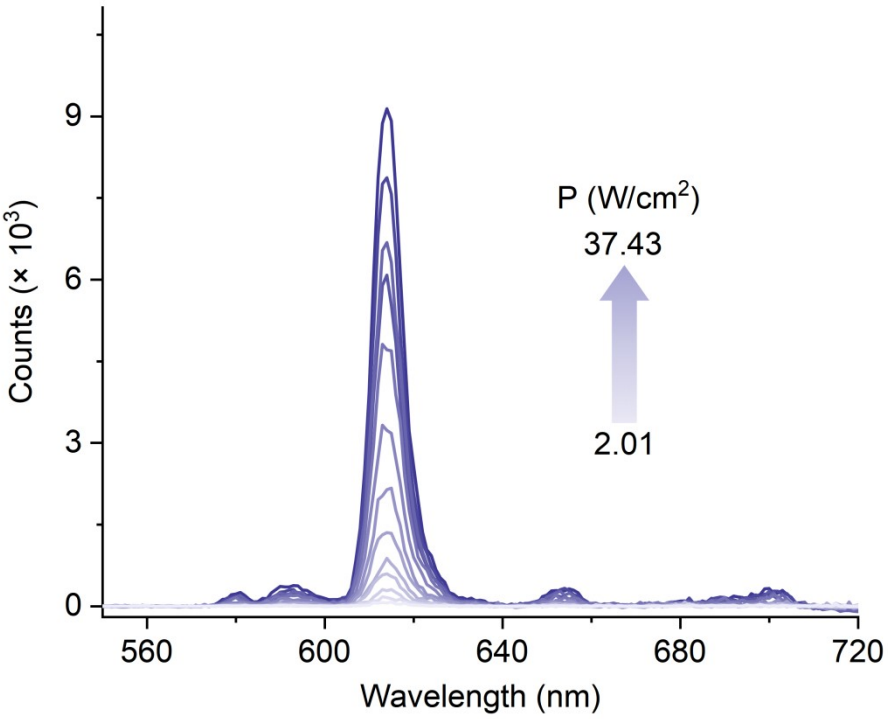

Figure S24. The UC emission spectra of $(Yb_{3.5}Eu_{0.5}\mathbf{L}_4)(R\text{-}BINAPO)_4$ in $CHCl_3$ with variable laser power (λ_{ex} = 980 nm, $c = 2.5 \times 10^{-3}$ M, Number of scans = 3).

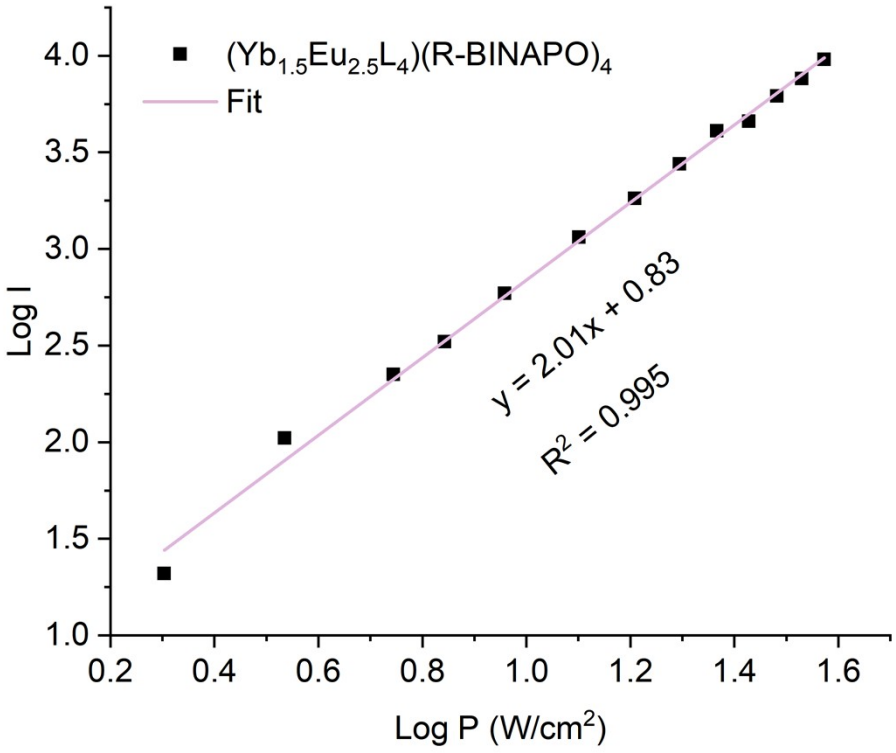

Figure S25. The log−log plots of the UC intensity integrated (I) from 570 to 720 nm of $(Yb_{1.5}Eu_{2.5}\mathbf{L}_4)(R\text{-}BINAPO)_4$ as a function of the laser power density P (in W cm^{-2}).

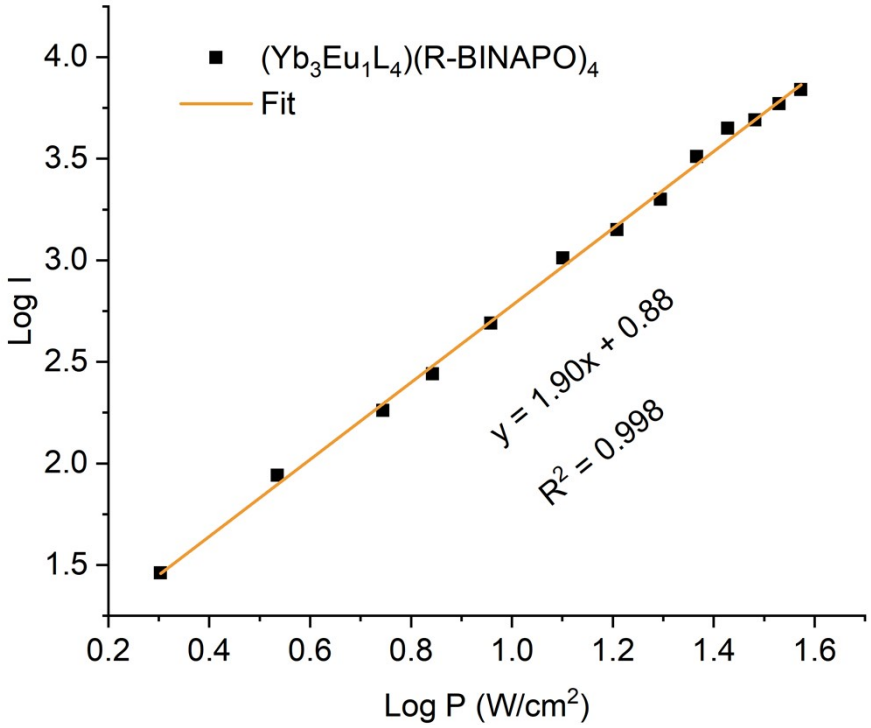

Figure S26. The log−log plots of the UC intensity integrated (I) from 570 to 720 nm of $(Yb_{3.0}Eu_{1.0}\mathbf{L}_4)(R\text{-}BINAPO)_4$ as a function of the laser power density P (in W cm^{-2}).

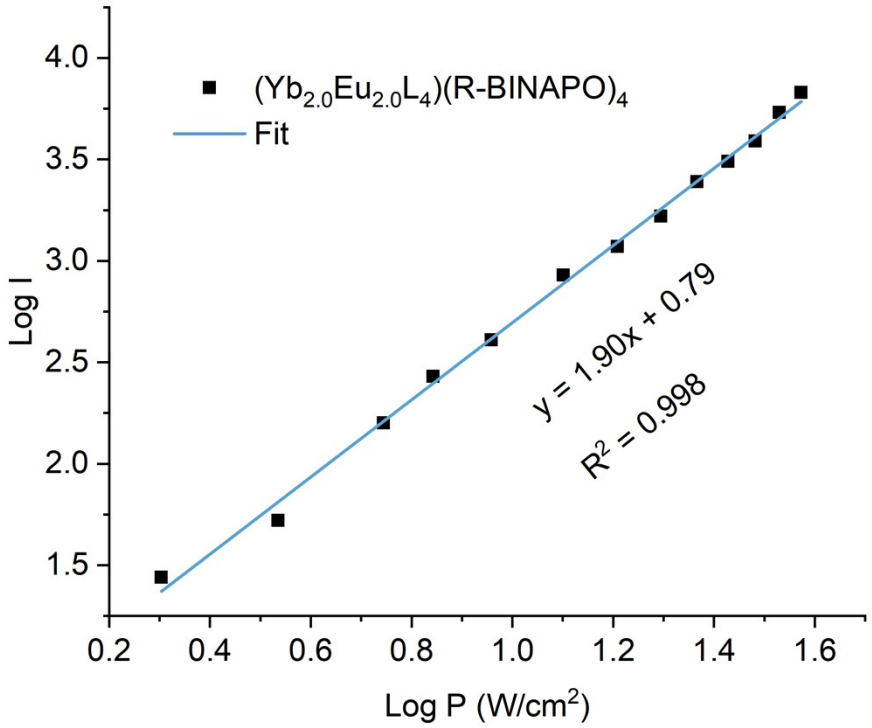

Figure S27. The log−log plots of the UC intensity integrated (I) from 570 to 720 nm of $(Yb_{2.0}Eu_{2.0}\mathbf{L}_4)(R\text{-}BINAPO)_4$ as a function of the laser power density P (in W cm^{-2}).

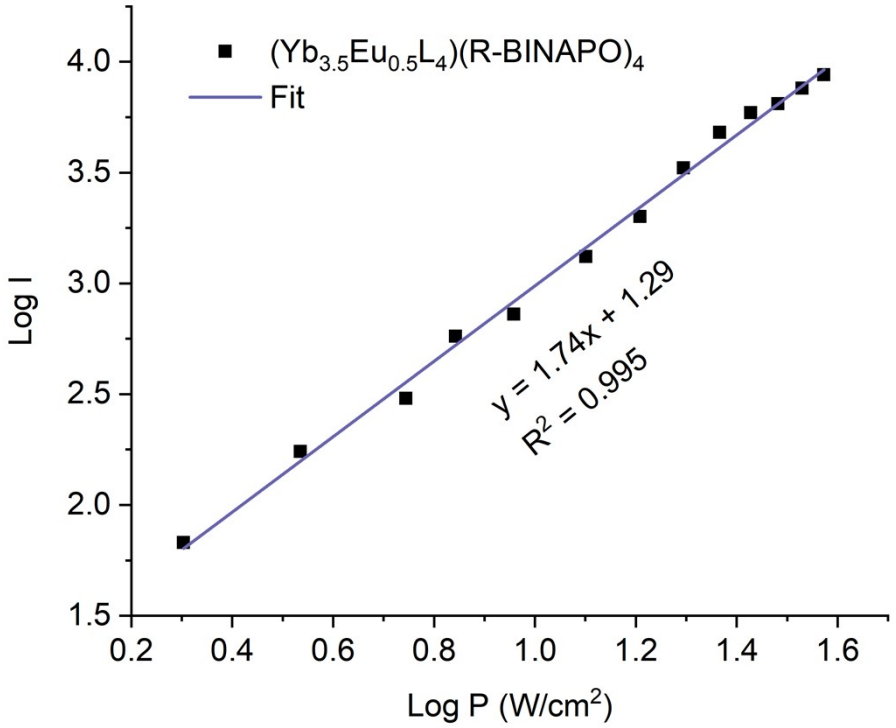

Figure S28. The log−log plots of the UC intensity integrated (I) from 570 to 720 nm of $(Yb_{3.5}Eu_{0.5}\mathbf{L}_4)(R\text{-}BINAPO)_4$ as a function of the laser power density P (in W cm^{-2}).

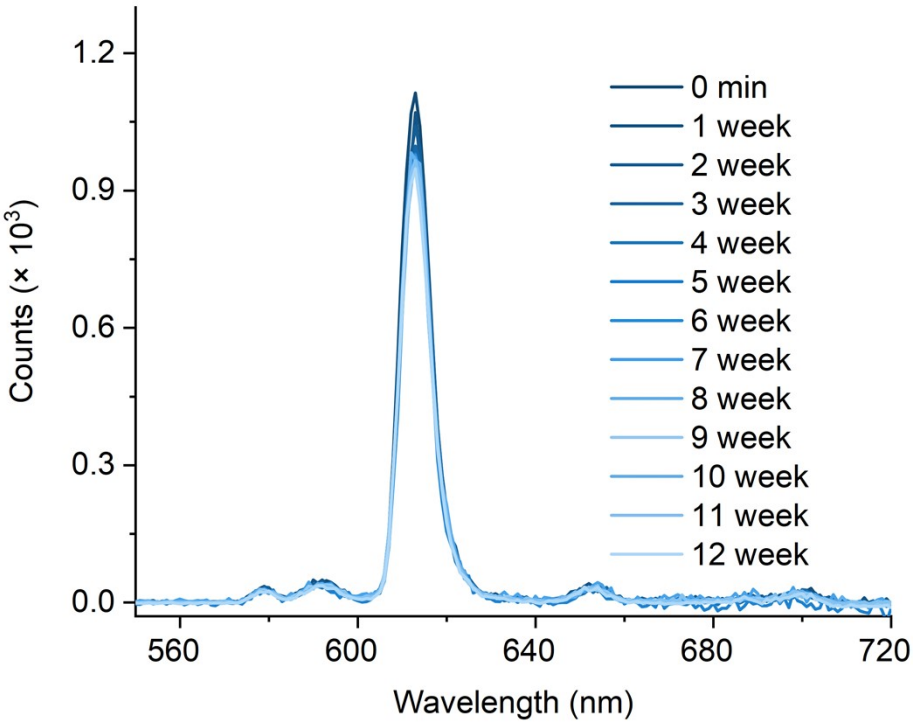

Figure S29. Upconversion luminescence spectra of $(Yb_{2.5}Eu_{1.5}\mathbf{L}_4)(R\text{-}BINAPO)_4$ in $CHCl_3$ (c = 2.5×10^{-3} M) assembly under 980 nm (P = 37.43 W cm^{-2}) excitation and after 3 months stored in an amber desiccator in the dark at room temperature. The two spectra were obtained using the same experimental conditions (emission slit and integration time).

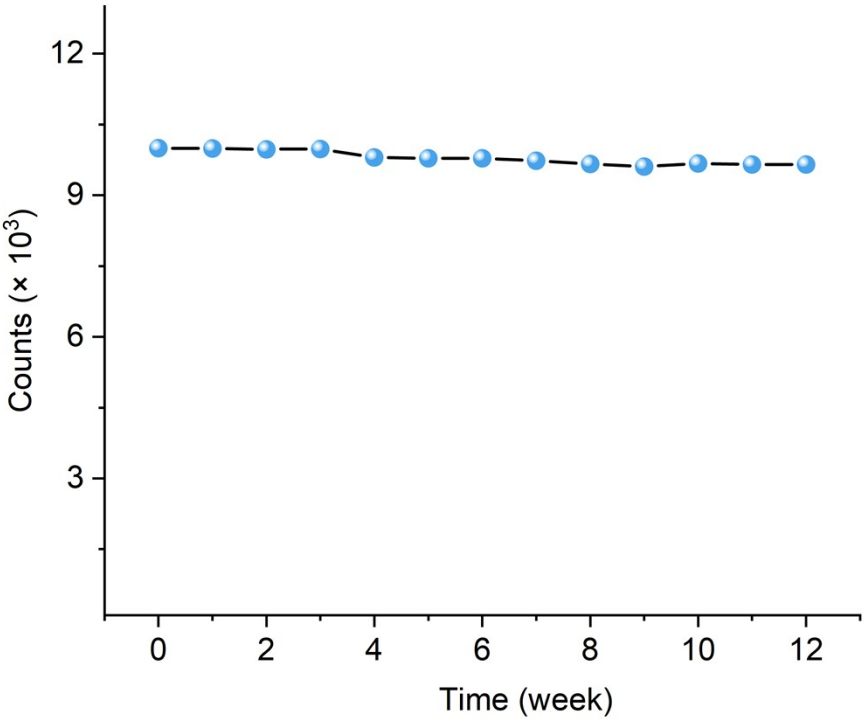

Figure S30. The emission intensity of $(Yb_{2.5}Eu_{1.5}\mathbf{L}_4)(R\text{-}BINAPO)_4$ versus time under 980 nm laser irradiation (P = 37.43 W cm $^{-2}$).

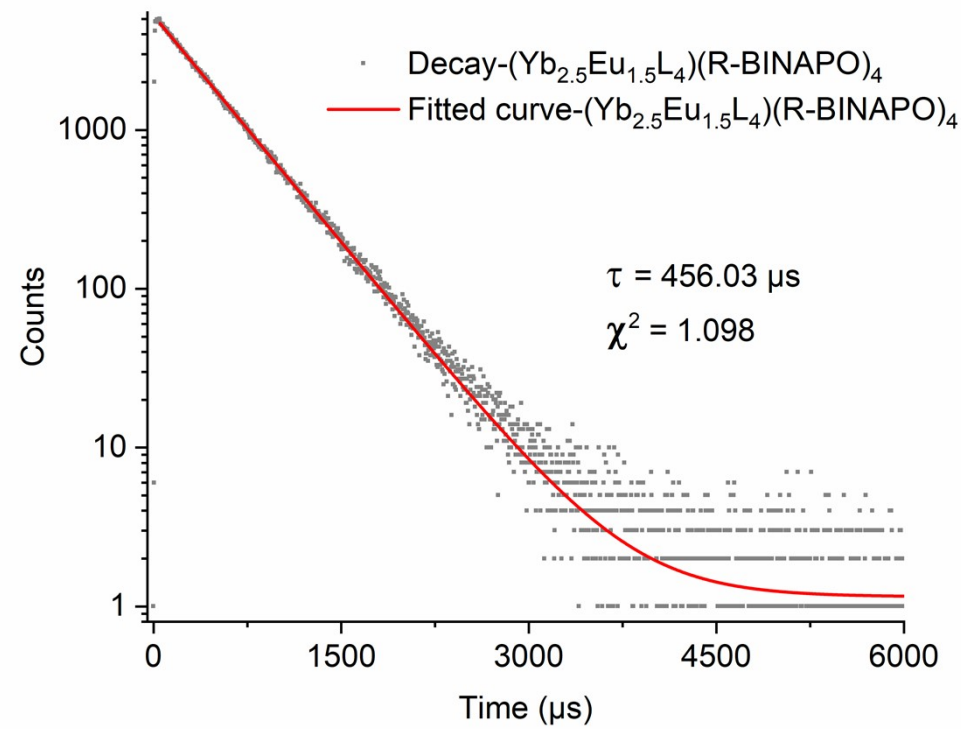

Figure S31. Luminescence decay curve of $(Yb_{2.5}Eu_{1.5}\mathbf{L}_4)(R\text{-}BINAPO)_4$ in $CHCl_3$ monitored at 612 nm (λ_{ex} = 395 nm).

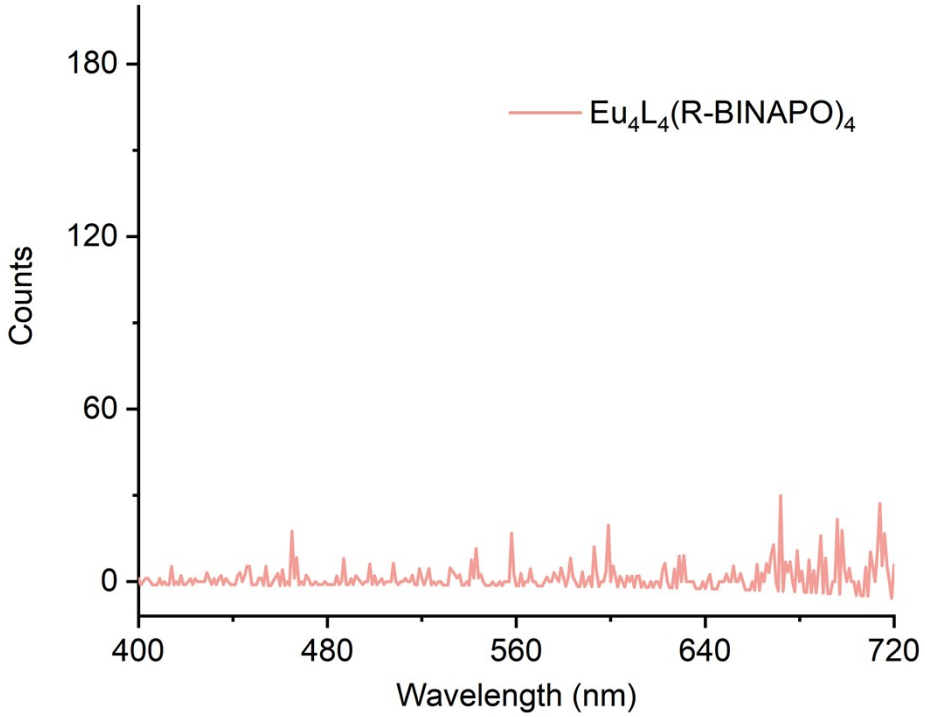

Figure S32. Upconverted emission spectrum of $Eu_4\mathbf{L}_4$(R-BINAPO)$_4$ in $CHCl_3$ (c = 2.5 × 10^{-3} M) upon excitation with 980 nm (P_{980} = 37.43 W/cm^2).

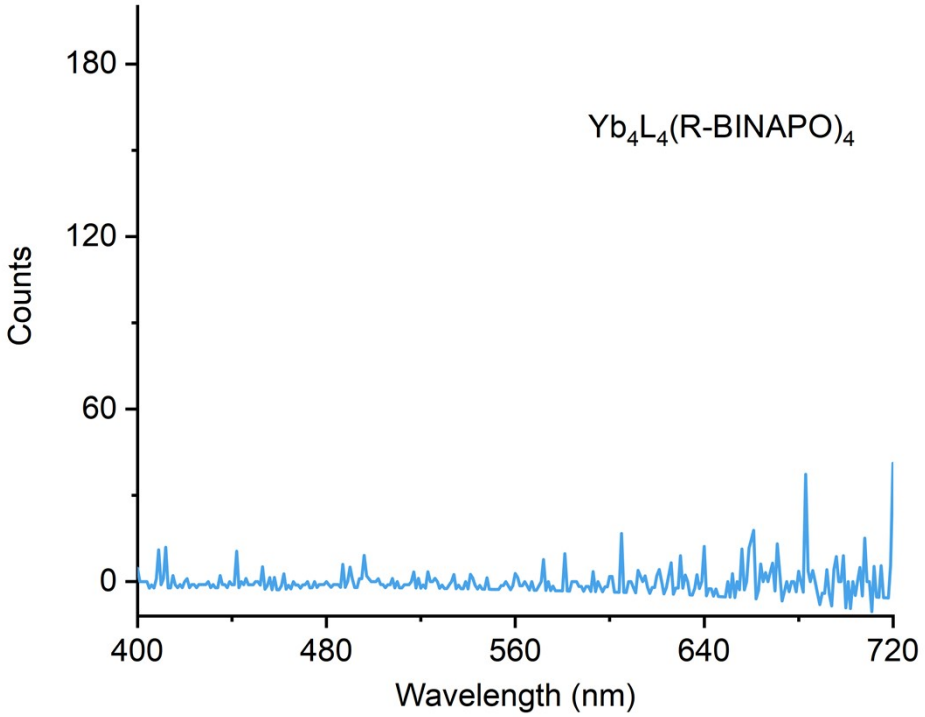

Figure S33. Upconverted emission spectrum of $Yb_4\mathbf{L}_4$(R-BINAPO)$_4$ in $CHCl_3$ (c = 2.5 × 10^{-3} M) upon excitation with 980 nm (P_{980} = 37.43 W/cm^2).

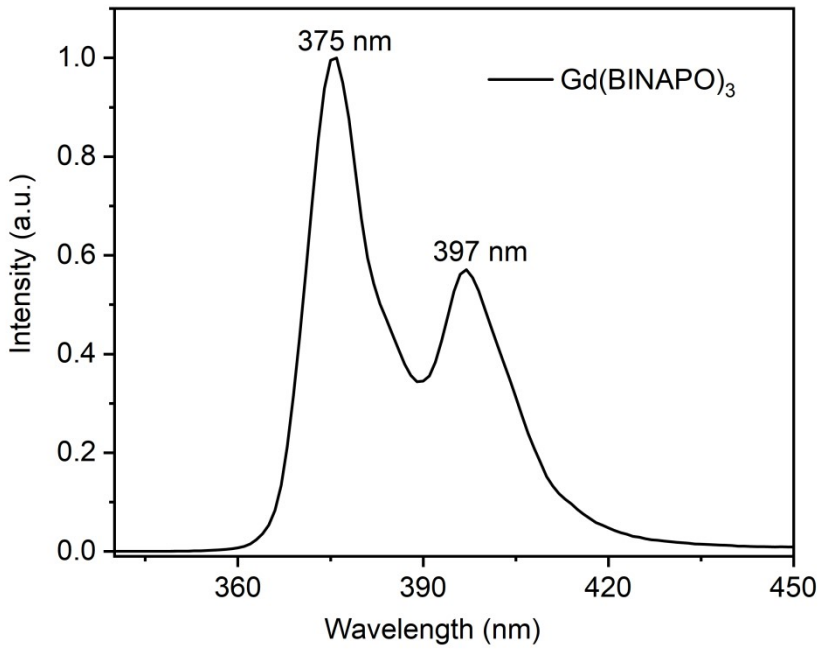

Figure S34. Phosphorescence spectrum of $Gd(BINAPO)_3$ in THF ($c = 1.0 \times 10^{-5}$ M) measured at 77 K.

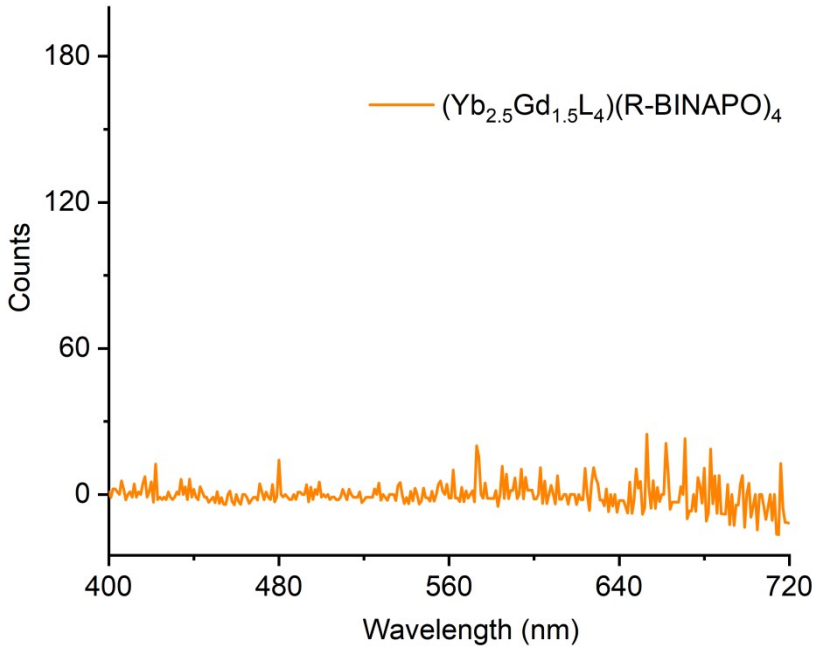

Figure S35. Phosphorescence spectrum of $(Yb_{2.5}Gd_{1.5}\mathbf{L}_4)(R\text{-BINAPO})_4$ in $CHCl_3$ ($c = 2.5 \times 10^{-3}$ M) upon excitation with 980 nm ($P_{980} = 37.43$ W/cm^2) measured at 77 K.

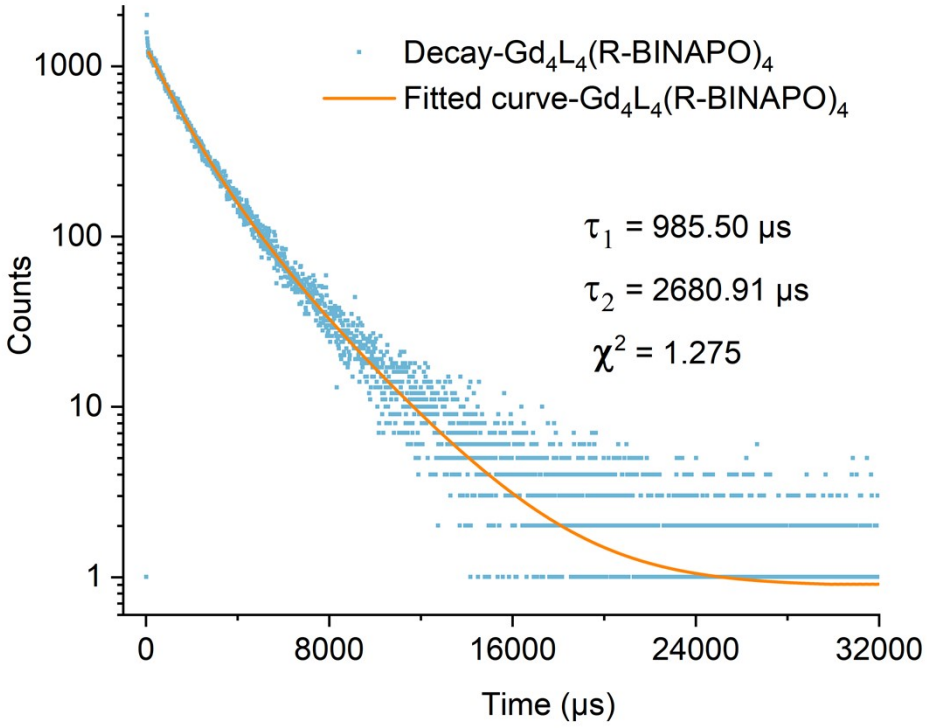

Figure S36. Luminescence decay curve of $Gd_4\mathbf{L}_4$(R-BINAPO)$_4$ in $CHCl_3$ (c = 1.0 × 10^{-5} M) monitored at 480 nm.

Table S2 The g_{lum} values at 595 nm for ($Yb_xEu_{4-x}\mathbf{L}_4$)(R-BINAPO)$_4$ (x = 0.5−3.5) in $CHCl_3$ (λ_{ex} = 980 nm, 2.5 × 10^{-3} M).

x/4-x	0.5/3.5	1.0/3.0	1.5/2.5	2.0/2.0	2.5/1.5	3.0/1.0	3.5/0.5
g_{lum}	−0.17	−0.18	−0.19	−0.19	−0.22	−0.19	−0.18

4. Calculation of the Proportions of Each Assembly

The component probability statistics for the assemblies comprising 2.5 equiv. of $Yb(OTf)_3$, 1.5 equiv. of $Ln(OTf)_3$ (Ln = Eu or Gd), 4 equiv. of **L** and 4 equiv. of R/S-BINAPO were calculated. For the sake of simplicity, Yb and Gd are denoted as A and B, respectively, with a ratio of A/B = 5/3. Assuming that A is 5n, then B is 3n. The specific calculation process is as follows:

$$T = C_{8n}^{4} = \frac{(8n)!}{4! \cdot (8n-4)!}$$

$$A_4 = C_{5n}^{4} = \frac{(5n)!}{4! \cdot (5n-4)!}$$

$$A_3B_1 = C_{5n}^{3} \cdot C_{3n}^{1} = \frac{(5n)!}{3! \cdot (5n-3)!} \cdot \frac{(3n)!}{1! \cdot (3n-1)!}$$

$$A_2B_2 = C_{5n}^{2} \cdot C_{3n}^{2} = \frac{(5n)!}{2! \cdot (5n-2)!} \cdot \frac{(3n)!}{2! \cdot (3n-2)!}$$

$$A_1B_3 = C_{5n}^{1} \cdot C_{3n}^{3} = \frac{(5n)!}{1! \cdot (5n-1)!} \cdot \frac{(3n)!}{3! \cdot (3n-3)!}$$

$$B_4 = C_{3n}^{4} = \frac{(3n!)}{4! \cdot (3n-4)!}$$

When $n \to +\infty$, the percentage contents of each component are as follows:

$$A_4(\%) = \frac{5^4}{8^4} = 15.26\%$$

$$A_3B_1(\%) = \frac{4 \times 5^3 \times 3}{8^4} = 36.62\%$$

$$A_2B_2(\%) = \frac{6 \times 5^2 \times 3^2}{8^4} = 32.96\%$$

$$A_1B_3(\%) = \frac{4 \times 5 \times 3^3}{8^4} = 13.18\%$$

$$B_4(\%) = \frac{3^4}{8^4} = 1.98\%$$

5. Calculation of the UC quantum yields

The UC quantum yields were quantified using the relative method with the known [$(YbL_1)_2Tb$] ($\Phi_{ref} = 1.4 \times 10^{-8}$ in D_2O at room temperature) as the reference. All measurements of reference compounds, including the NIR absorption and UC emission spectra, have been performed on the same spectrometer and under the exact same test conditions (P_{980} = 37.43 W/cm^2) as the compounds in this paper mentioned.

Quantitative data in dilute solutions (A < 0.05) were obtained from the following equation:

$$\frac{\Phi_{up}}{\Phi_{ref}} = \frac{E_{up}}{E_{ref}} \cdot \frac{A_{ref}}{A_{UC}} \cdot \frac{n_{ref}^2}{n_{up}^2} \cdot \frac{P_{exc,ref}}{P_{exc,up}} \cdot \frac{h\nu_{exc,up}}{h\nu_{exc,ref}}$$

Where, Φ is the quantum yield, E is the integrated emission intensity (The integral area of the emission spectrum), A is the absorbance at the excitation wavelength λ (λ = 980 nm), n is the refractive index (n($CHCl_3$) = 1.446 and n(D_2O) = 1.328), P_{exc} is the power intensity of the excitation source, h is the planck constant and ν_{exc} is the frequency of excitation wavelength.

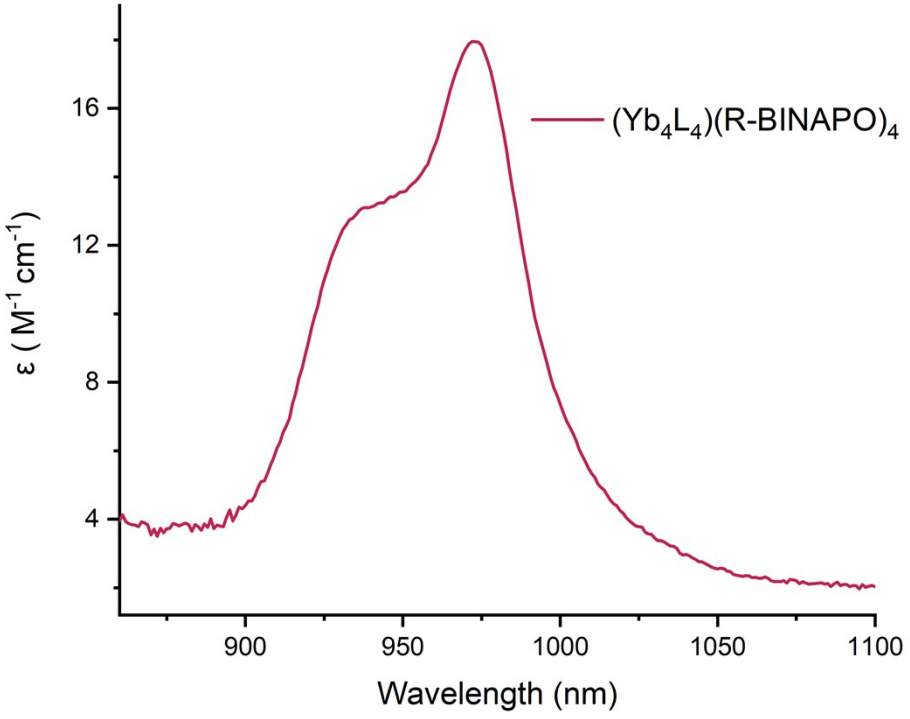

Figure S37. NIR absorption spectrum of (Yb_4**L**$_4$)(R-BINAPO)$_4$ (c = 2.5 × 10^{-3} M) in $CHCl_3$.

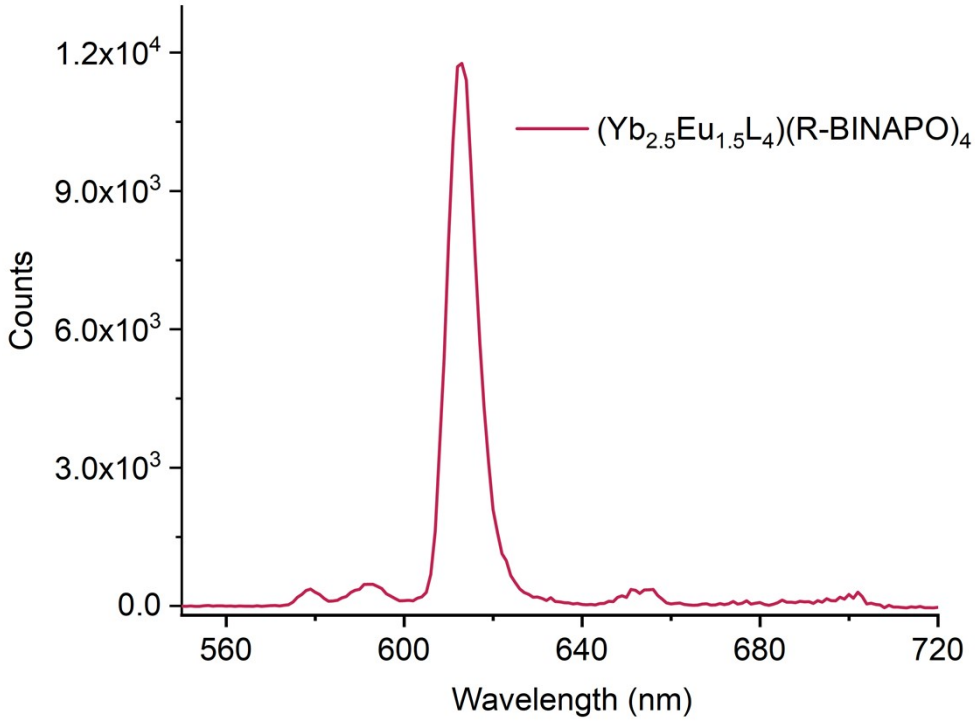

Figure S38. The UC emission spectrum of $(Yb_{2.5}Eu_{1.5}\mathbf{L}_4)(R\text{-}BINAPO)_4$ in $CHCl_3$ (c_{Yb} = 1.00 × 10^{-3} M, $CHCl_3$, P_{980} = 37.43 W/cm^2). The integral area of the emission spectrum from 560 to 720 nm is 1.69 × 10^5 (Number of scans = 1). The absorbance at 980 nm in a 1 cm cuvette was calculated as $A = \varepsilon \cdot c \cdot l = 4.02 \times 1.00 \times 10^{-3} \times 1 = 4.02 \times 10^{-3}$.

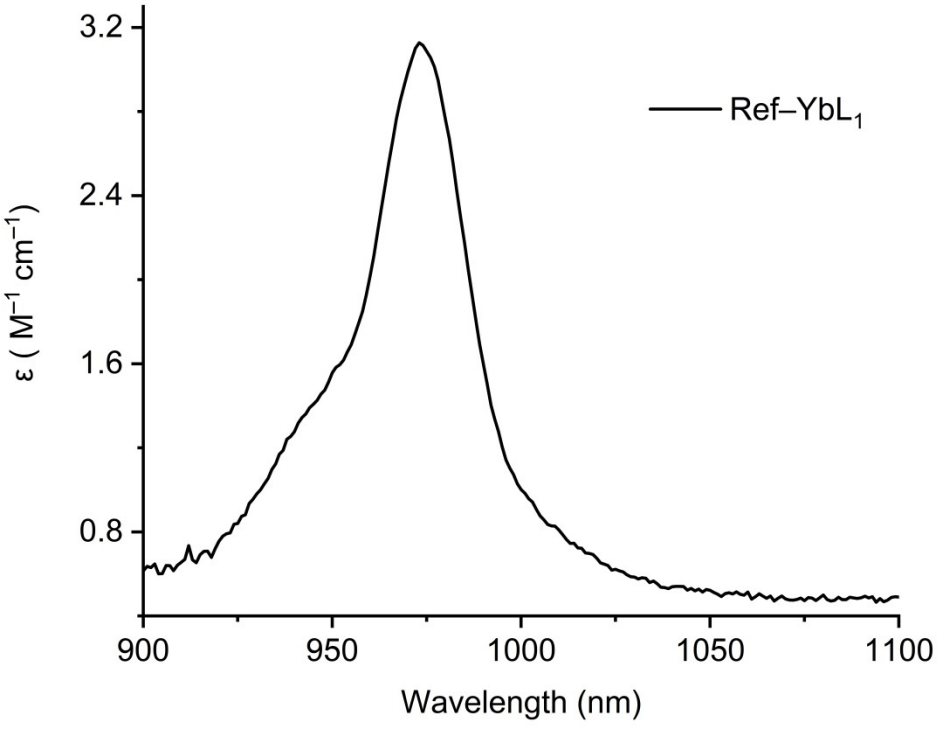

Figure S39. The NIR absorption spectrum of reference compound YbL_1 in D_2O.

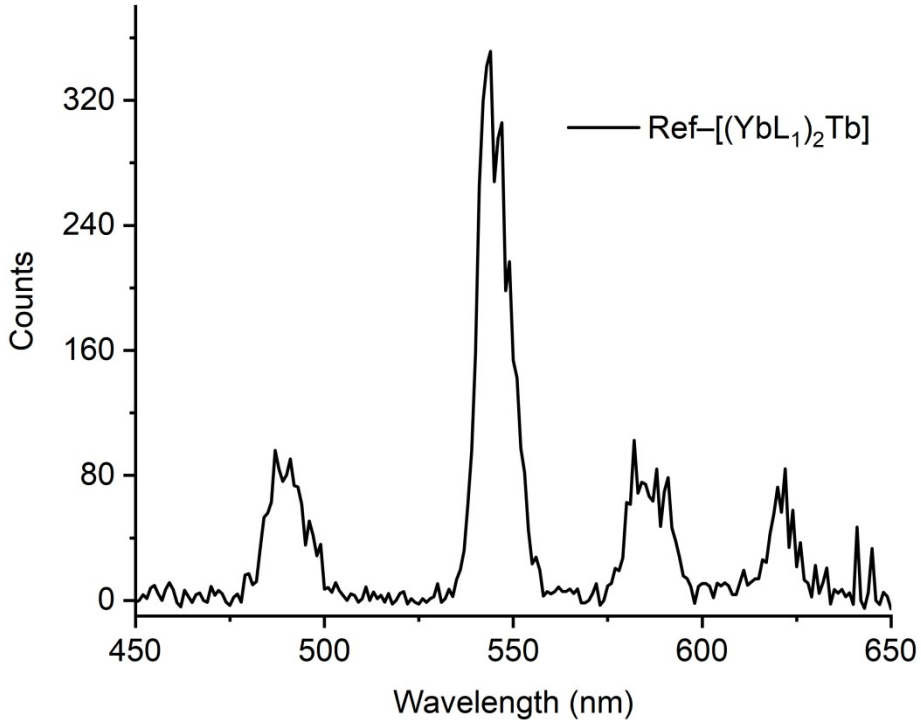

Figure S40. The UC emission spectrum of $[(YbL_1)_2Tb]$ in D_2O (c_{Yb} = 6.00 × 10^{-3} M, P_{980} = 37.43 W/cm^2). The integral area of the emission spectrum from 450 to 650 nm is 6.84 × 10^3 (Number of scans = 3), which corresponds to 2.28 × 10^3 for a single scan (NS = 1). The intensity at the maximum (544 nm) is 3.51×10^2. The absorbance at 980 nm in a 1 cm cuvette was calculated as $A = \varepsilon \cdot c \cdot l = 2.67 \times 6 \times 10^{-3} \times 1 = 1.60 \times 10^{-2}$.

Finally, the quantum yield of the tetrahedral cage $(Yb_{2.5}Eu_{1.5}\mathbf{L}_4)$(R-BINAPO)$_4$ was derived by the relative method as 3.50 × 10^{-6}.

6. References

1 Agilent Technologies, *CrysAlisPro v.* 1.171.36.28, 2013.
2 O. V. Dolomanov, L. J. Bourhis, R. J. Gildea, J. A. K. Howard and H. Puschmann, *J. Appl. Crystallogr.*, 2009, **42**, 339−341.
3 G. M. Sheldrick, *Acta. Crystallogr. A.*, 2008, **64**, 112−122.
4 A. L. Spek, *J. Appl. Crystallogr.*, 2003, **36**, 7−13.